PCCP

Accepted Manuscript

ROYAL SOCIETY OF CHEMISTRY

www.rsc.org/pccp

Physical Chemistry Chemical Physics
CREATED USING THE RSC LaTeX PCCP ARTICLE TEMPLATE – SEE www.rsc.org/electronicfiles FOR DETAILS

ARTICLE TYPE www. rsc.org/xxxxxx | XXXXXXXX

Strong field control of photochemistry

Ignacio Solá,[a] Jesús González-Vázquez,[b] Rebeca de Nalda,[c] and Luis Bañares[a]

Received Xth XXXXXXXXXX 20XX, Accepted Xth XXXXXXXXX 20XX
First published on the web Xth XXXXXXXXXX 200X
DOI: 10.1039/b000000x

Strong ultrashort laser pulses have opened new avenues for the manipulation of photochemical processes like photoisomerization or photodissociation. The presence of light intense enough to reshape the potential energy surfaces may steer the dynamics of both electrons and nuclei in new directions. A control laser pulse, precisely defined in terms of spectrum, time and intensity, is the essential tool in this type of approaches to control chemical dynamics at a microscopic level. In this Perspective we examine the current strategies developed to achieve control of chemical processes with strong laser fields, as well as recent experimental advances that demonstrate that properties like the molecular absorption spectrum, the state lifetimes, the quantum yields or the velocity distributions in photodissociation processes can be controlled by the introduction of carefully designed strong laser fields.

Ignacio Sola received his Ph.D. in Chemistry from Universidad Complutense de Madrid (UCM) in 2000. After a postdoctoral stay in Princeton University he became assistant professor (2004) and then associate professor (2007) in the Department of Physical Chemistry at UCM. He is mainly interested in understanding the dynamics of quantum systems under ultrastrong and ultrafast laser pulses, setting the limits on what and how molecules can be controlled by light, and in applying these insights in functionalizing molecules as nanoscopic devices, for use in chemical reactions or as information drivers.

Jesús González-Vázquez received his Ph.D. in Theoretical and Computational Chemistry from Universidad Complutense de Madrid in 2007. He held postdoctoral positions at the Freie Universtät Berlin (2007-2008), the Friedrich-Schiller-Universität Jena (2008-2009) and the Instituto de Química Física "Rocasolano" at CSIC Madrid under the "Juan de la Cierva" program (2010-2012). Since 2013, he is a postdoc at Universidad Autónoma de Madrid under the framework of the ERC project XCHEM.

Rebeca de Nalda received her Ph.D. in Physics from Universidad Complutense de Madrid (UCM) in 1999. She held postdoctoral positions first in the Optics Institute of CSIC (National Research Center, Spain), and later in Imperial College London (UK) as a research associate. She obtained a tenure-track "Ramón y Cajal" contract in UCM and in 2005 became permanent scientific staff of the Instituto de Química Física "Rocasolano" at CSIC. Her research interests are centered on the behavior of matter under laser radiation, mainly at high intensities and short temporal scales, both in the gas phase and in solid materials.

1 Introduction

Dynamic control of chemical reactions or photochemical processes has only been possible with the development of laser technology.[1–14] Two different avenues were followed initially. On one hand, adiabatic control[15,16] and coherent control[17] emerged from non-linear high-finesse spectroscopic techniques. For instance, quantum control is needed to improve the yield of a Raman transition avoiding fluorescence in the stimulated Raman adiabatic passage (STIRAP) scheme of Eberly and coworkers[18] and Bergmann and coworkers.[19] It is also needed to select a target state from a set of degenerate quantum states in the coherent control schemes of Brumer and Shapiro.[20] Basically, the relative phase between the pulses and the sequence by which isolated Hamiltonian resonances act in the dynamics play the essential role in determining the outcome of the desired molecular process, which is pre-designed by the controller. The control is thus exerted mainly in the frequency domain, by focusing several phase-locked laser beams or designing specific sequences of pulses. Interesting theoretical concepts, like the dressed states, have their roots in these original ideas. On the other hand, pump-dump control[21] or quantum optimal control theory[22,23] and adaptive learning control[24] emerged from the development of ultrafast dynamics spectroscopy.[25] The key idea is the generalization of the pump-probe scheme. As is well known, pump-probe spectroscopy is based on an ultrafast (typically femtosecond) pump pulse that photo-initiates the dynamics in the Franck-Condon region of a molecular electronic excited state, followed by a second (possibly) ultrafast pulse, time-delayed with femtosecond time precision, that probes the evolution of a wave packet as it travels along the reaction coordinate.[26,27] But pump-probe pulses can be used for purposes other than spectroscopic; they can be designed to induce a particular dynamical response in the molecule. In the simplest Tannor and Rice scheme,[21] this response is selected by controlling the time-delay of the pulses. While scanning different time-delays allows to characterize the "full movie" of the dynamics of the wave packet, one can single-out a particular frame, where the wave packet is located at the desired position. Typically then the probe pulse is in fact a dump pulse that partly restores the chosen wave packet on the ground state. In any case, the control here requires using strong probe pulses, as one does not seek to trace but rather to move the population. Experimentally, the assessment of the yield of the process may require an additional third laser that should work as a proper probe of the control.

A first step towards putting both traditions together was conceived by making the pump, rather than the probe (or dump), the main control driver. An ultrashort, minimal time-width pulse implies a transformed-limited maximally coherent pulse, but the phase relation between different spectral components can be manipulated in pulse-shapers, inducing temporal profiles in the pulses as complex as demanded.[28–30] In the simplest case, the phase varies quadratically in time, inducing what is called a linear chirp (the instantaneous frequency changes linearly from red to blue or blue to red as the pulse proceeds). In the adiabatic rapid passage (ARP) scheme[15,16] the yield of an optical transition is greatly enhanced using chirped pulses where the frequency sweeps across the resonance. Other phases have been used to modulate, mask certain frequencies or split the original pulse into sub-pulses.[31–33] In more complex systems the key to control the dynamics is entailed in the constructive and destructive interfering processes of the system dynamics. For instance, several frequency components can work in parallel with certain phase relationships, as in the Brumer-Shapiro scheme.[17] In general, in order to synchronize the multispectral nature of the Hamiltonian dynamics with respect to the pulse characteristics, quantum optimal control theory has been proposed[7,8,22,34]. In all these schemes a phase and/or amplitude modulated pulse is the main control tool. In most practical cases, techniques such as mass spectrometry[35,36], laser-induced fluorescence, resonance enhanced multiphoton ionization (REMPI), photoelectron spectroscopy[37,38], ion imaging[38], or photoelectron photoion coin-

Luis Bañares received his Ph.D. in Chemistry from Universidad Complutense de Madrid (UCM) in 1990. Following postdoctoral research associate positions at California Institute of Technology and Universität Würzburg with Fulbright and Alexander von Humboldt fellowships, respectively, he joined UCM as an assistant professor, associate professor and since 2007 as a full professor. He is the director of the Center for Ultrafast Lasers at UCM. His research interests are related to experimental and theoretical chemical reaction dynamics and femtochemistry. His work focuses on the understanding of fundamental chemical reactions and photodissociation processes at a molecular level.

[a] *Departamento de Química Física I (Unidad Asociada de I+D+i al CSIC), Facultad de Ciencias Químicas, Universidad Complutense de Madrid, 28040 Madrid, Spain. Fax: +34 913944135; Tel: +34 913944228; E-mail: lbanares@ucm.es*

[b] *Departamento de Química, Módulo 13, Universidad Autónoma de Madrid, 28049 Madrid, Spain.*

[c] *Instituto de Química Física Rocasolano, CSIC, C/ Serrano, 119, 28006 Madrid, Spain.*

cidence imaging[39,40], were used as probes of the process to be controlled. A most effective experimental set-up, usually referred to as adaptive learning, was proposed by Rabitz *et al.*; it consists of coupling the pulse-shapers that modulate the control pulse with learning algorithms that retrieve the information from the probe in a closed-loop design.[24] In the last fifteen years, many experimental results in the laser control of photofragmentation of complex molecules[10,34,41–48] or control of photochemistry in the condensed phase[49–51] have validated this idea, but the challenge remains in interpreting the control mechanisms that lead to the general efficiency of the method.[42,48,50,52–55].

Besides the time or frequency domain features of the pulses, the laser intensity constitutes another essential control knob that is recently gaining a leading role in new control scenarios. Beyond intensities larger than the TW cm^{-2}, nonlinear multiphoton transitions may occur. Additionally, Autler-Townes resonances[56] and strong Stark shifts[57,58] modify the electronic forces and reshape the potential energy surfaces. Static phenomena like bond hardening in a laser-free dissociative state[59] or bond softening of the ground state[60] were first observed and interpreted theoretically through concepts like the light-induced potentials or LIPs.[61–64] Many schemes were devised for selective transfer of vibronic population through the LIPs, as in the adiabatic passage by light-induced potentials (APLIP) scheme[63,65–70], sometimes with the use of chirped pulses, as in the chirped adiabatic rapid passage (CARP)[71–73] and by a sequence of non-resonant pulses or through resonance, as in the selective population of dressed states (SPODS) scheme.[74–77] In addition to selective excitation, schemes were conceived to control other molecular properties or functions, as the adiabatic squeezing of the nuclear wave function[78], the controlled elongation of the bond distance, as in the laser adiabatic manipulation of the bond (LAMB) scheme[79–86] or the control of intramolecular transitions in the molecule, whether induced by spin-orbit couplings (intersystem crossing)[87–90] or via nonadiabatic couplings (internal conversion).[91] Schemes based on preparing coherent superpositions of electronic states, inducing "charge-directed reactivity" through subfemtosecond tailoring of the light electric field have been excellently reviewed recently[92] and fall beyond the scope of the present article.

Most of the aforementioned schemes require the use of two-to-several strong fields, all of them implied in the control of the dynamics. The main challenge in applying the schemes lies in the need for selecting a very specific channel (typically a two-photon transition) from the set of all possible quantum pathways opened by the strong field couplings. Although strong fields can be used to control ionic channels,[93–97] in the case of control of neutral states they will certainly produce unwanted multiphoton processes that can reduce the yield of the desired transition. Moreover, phenomena like multiphoton ionization, field ionization and Coulomb explosion will hinder the success of the selected process. Hence the need for working in the subtle regime of so called moderately intense laser fields. On the other hand, if one can disentangle the dynamics of the ion from the dynamics of the neutral molecule, the ionization process can be used as a probe of the dynamics, saving the necessity of using another laser as the probe. Additionally, strong laser pulses may induce alignment (and sometimes orientation) in the molecule[57,98–100], which not only facilitates the control of the stereodynamics of the process, but may also avoid the average of the yield as a function of the orientation of the molecule with respect to the laser polarization.

An important experimental advance in the development of moderately strong laser control strategies came with the introduction of a scheme based on three laser pulses, the pump pulse, igniting the dynamics, the ancillary strong field, controlling the motion, and the probe pulse, diagnosing the outcome of the process. The first application was the control of a photochemical reaction. In the nonresonant dynamic Stark effect (NRDSE) scheme of Sussman, Stolow and coworkers,[57,101–104] the control pulse is a strong femtosecond IR field that affects the photodissociation dynamics by Stark shifting the excited electronic states while the wave packet dissociates, causing changes in the branching ratio of the reaction. One advantage of the NRDSE approach is its universality. There is no need to drive the photodissociation reaction through other excited states, that is, via other transition states. Therefore the frequency of the control pulse does not need to be tuned to a particular resonance. However, one may still need to avoid multiphoton resonances. Pulses with wavelengths around one micrometer or longer are expected to maximize the success of the scheme.

Instead of using nonresonant fields, the control pulse can be tuned to a particular transition. Since the pulse is strong, even very weak transitions as, for instance, one-photon excitation of scattering or continuum states, can be induced by the control pulse. Considering the orientation of the field with respect to the induced transition dipole as an additional degree of freedom makes this resonant process a light-induced conical intersection (LICI) even in diatomic molecules[105–110] and in polyatomic molecules[111].

Very recently, control via LICIs has been used to manipulate the yield of a photoisomerization reaction[112] and a direct photodissociation process[113], allowing in the latter case an efficient breaking of the bond in the ground electronic state. Although photodissociation in the ground state can often be achieved through internal conversion, it is hardly accessible by optical transitions, *i.e.* it is hardly controllable. A further step is required to manipulate the velocity of the fragments. In order to change the asymptotic fragment kinetic energy distribution, the effect of the control field must be large enough. Therefore, it needs to affect a larger region of the potential

energy surfaces around the LICI. In addition one must break the adiabatic motion of the wave packet through the LIP, so that abrupt changes in the momentum are impinged in the final distribution. The ability to manipulate changes on the wave packet momentum are equivalent to the ability to force "changes in the representation" of the wave packet, from the adiabatic to the diabatic representations. Together with the precise creation of conical intersections (or avoided crossings) with a laser pulse, as in a LICI, these tools can be used to experimentally simulate the dynamics in processes of internal conversion, which are notoriously difficult to follow in real time. The pump plus Stark-shift-control plus probe scheme, shows great promise in the control of molecular alignment and reaction ratios and kinetic energy distributions of the products in photodissociation reactions with competing photochemical processes, such as intersystem crossing or internal conversion. An example of the degree of control that can be achieved in a direct photodissociation reaction was recently shown in a polyatomic molecule, CH_3I, for the first time. [113]

The developments in recent years have stimulated a great deal of new experiments in the quantum control community, of which the previous paragraphs only show a glimpse. In this Perspective, we will focus on the control induced by strong (ultrashort) laser fields on photochemical processes with emphasis on photodissociation reactions. After presenting the main models and strategies for strong field control, we will present representative recent examples of experimental work on strong field control over absorption spectra, quantum yields, lifetimes and the velocity of the fragments in a dissociation process. Some future directions of the strong field control of photochemical processes will be given at the end.

2 Strategies for strong field control of photochemistry

2.1 Dynamic Stark effect

As a starting point, we assume for simplicity that only two Hamiltonian eigenstates ($\hat{H}\phi_j = E_j\phi_j$) contribute to the dynamics, $\psi(t) = \sum_j c_j(t)\phi_j$ ($j = 1,2$). In the length gauge, the coupling between the molecule and the laser field is given by the dipole interaction $V_{\rm int} = -\vec{\mu}_{12}\cdot\vec{E}(t)$, where $\vec{\mu}_{12}$ is the transition dipole between both coupled states and $\vec{E}(t)$ is the laser field vector. Both magnitudes are vectors. Separating terms with different time dependences, $V_{\rm int} = -\vec{\mu}_{12}\cdot\vec{\varepsilon}\mathscr{E}(t)\cos(\omega t)$, where $\vec{\varepsilon}$ is the laser polarization unit vector, $\mathscr{E}(t)$ a slow envelope function and ω is the pulse carrier frequency. Here we are considering that the pulse is long enough (10 or more optical cycles) so that its spectral width is much smaller than the carrier frequency. In the matrix representation of the Hamiltonian eigenstates and using the rotating wave approximation (RWA), [114,115] which basically assumes that the time-scale of the dynamics of the system (at the level of the description) is much larger than ω^{-1}, the Hamiltonian matrix $\mathbf{H}$ is

$$\mathbf{H} = \begin{pmatrix} 0 & V_{\rm int}(t)/2 \\ V_{\rm int}(t)/2 & \Delta \end{pmatrix} \qquad (1)$$

where $\Delta = E_2 - \hbar\omega$ is the energy detuning and we have conveniently chosen the energy of the initial state as the zero energy (or equivalently, we have made an appropriate global phase transformation of the wave function). $V_{\rm int}(t)$ lies in the off-diagonal of Eq. (1) and is thus directly responsible for the transition rate of population transfer between the states, particularly when the laser is on-resonance and $\Delta = 0$. Then the time-scale of population inversion is inversely proportional to the coupling, and one defines the Rabi frequency, $\Omega(t) = \mu_{12}\mathscr{E}(t)/\hbar$ (in units of frequency), which is the natural frequency at which the system responds to the radiation. Thus quantum control schemes typically use resonant transitions that make full use of controlling the rate at which particular transitions occur, allowing then for possible interference between different transitions that occur at the same time, or to time-order specific sequences of desired transitions.

Whenever Δ is small (in comparison to $V_{\rm int}$), one can define an effective Rabi frequency $\Omega_{\rm eff} = \sqrt{(\Omega^2 + \Delta^2)}$ and study the system dynamics in terms of $\Omega_{\rm eff}$. Now the rate of population transfer increases but the maximum population transfer is proportional to $\Omega^2/\Omega^2_{\rm eff}$, always smaller than one. However, when Δ is very large and the probability of finding the system in the excited state is very small, it becomes simpler to follow the dynamics by focusing only on the initial state. By adiabatic elimination of the second state of the Hamiltonian (implying $\dot{c}_2(t) \approx 0$) one obtains

$$\hat{H}_{\rm eff} = -\frac{\hbar^2}{4\Delta}\Omega^2(t) \qquad (2)$$

which means that the energy of the initial state decreases (and is modulated) by the square of the field, and depends as well on the detuning. This is the dynamic Stark effect.

In the description given by Eq. (2) the Hamiltonian only includes a single state, the initial one, whose energy varies in time. However, not only the energy but also the *nature* of this state is changing due to the inherited contribution of the second state. Thus, if one measures some other property that originally could be used to identify state ϕ_2 over state ϕ_1 (e.g., its angular momentum) then one could find some probability of measuring exactly the property assigned to the excited state.

As Δ becomes much smaller than ω, typically many different states, rather than just one [as in Eq. (1)], contribute to the dynamic Stark effect, since the energy separation between the excited states (the states not explicitly included in the dynamics of the system) becomes of the order or smaller than Δ. Then instead of writing the effective Hamiltonian in terms of

$\Omega^2(t)$, or $\mu_{12}^2\mathscr{E}^2(t)$, it is usual to describe the system in terms of the dynamic polarizability α,

$$\hat{H}_{\rm eff} = -\frac{1}{4}\alpha\mathscr{E}^2(t) \tag{3}$$

where

$$\alpha = \sum_j \frac{\mu_{1j}\mu_{j1}}{E_j - E_1 - \hbar\omega} \tag{4}$$

can be obtained by second order perturbation theory or other approaches. In Eq. (4) we only consider one contribution of the field to the polarizability (the $-\hbar\omega$ term in the denominator), consistent with the RWA. In fact, if $\omega \ll E_j - E_1 \; \forall j$ then one typically uses the static polarizability to describe this effect.

The same procedure used here to show how the energy of the ground state is Stark-shifted can be used to consider how the energy of excited states can be affected. But while the energy in the ground state always decreases as Eq. (2) shows (or similarly the sign of α is always positive in the ground state), the polarizability can be positive or negative in excited states. Therefore, the use of nonresonant strong fields can be used to control the energy of the different states without changing their populations. This is mainly a *structural* control of the system, by which the spectra is Stark-shifted. But the control is performed only during the time at which the laser operates. In this work we review processes that imply strong Stark-shifts requiring the use of ultrashort pulses (both because of the needed intensities and to avoid ionization). As we will see when considering the Hamiltonian of molecules in more detail, the control of the spectra especially in excited states implies *molecular deformation* and is a doorway to control many photochemical processes. As excited states show different intermolecular couplings and some of these couplings are relatively localized, by Stark shifts one can avoid or displace avoided crossings or conical intersections and affect for instance the lifetime of predissociative states or the rate of photochemical processes.

Before we concentrate on typical molecular problems we will consider another general control scenario. In this case, we assume two relatively close-lying states. Allowing in general for time-dependent frequencies (chirped pulses), whenever the pulse $\mathscr{E}(t)$ is on resonance at a particular time, then $\Delta(t) = E_2 - E_1 - \hbar\omega(t) = 0$. But additionally, both states ϕ_1 and ϕ_2 may be affected in a nonresonant way by the remaining more decoupled states of the system. Applying the RWA, the effective Hamiltonian of the system can be generally written as

$$\mathbf{H}_{\rm eff} = \begin{pmatrix} -\alpha_{11}\mathscr{E}^2(t)/4 & -\mu_{12}\mathscr{E}(t)/2 \\ -\mu_{12}\mathscr{E}(t)/2 & \Delta(t) - \alpha_{22}\mathscr{E}^2(t)/4 \end{pmatrix} \tag{5}$$

In Eq. (5), α_{jj} is a dynamic quasi-polarizability that contains the effect of the states not explicitly included in the Hamiltonian. In general, instead of a one-photon coupling between ϕ_1 and ϕ_2, these states can be coupled by a resonant or quasi-resonant two-photon process, $\alpha_{12}\mathscr{E}^2$, or multiphoton processes. Then the detuning must take into account the number of photons n involved in the transition, $\Delta(t) = E_2 - n\hbar\omega$. Sometimes even two different pulses can be used: one causing the resonant coupling and another inducing a nonresonant effect, and more complex situations may arise when more than two states and different number of photons are involved. A usual frame for regarding the effect of the pulses by shifting the energies of the states with the appropriate number of photons is generally called a Floquet representation and we shall adopt the same name here, even when in most cases we will refer to the simplest scenario involving two states (or electronic potentials) coupled by a single photon.

In any case, one can define an effective detuning

$$\Delta_{\rm eff} = \Delta(t) - \frac{1}{4}(\alpha_{22} - \alpha_{11})\mathscr{E}^2(t) \tag{6}$$

that takes into account the degree of control on the relative energy between the states.

We will consider tw,o cases here. In the first one μ_{12} is weak. Even when $\Delta \neq 0$, the pulse $\mathscr{E}(t)$ (or an additional pulse) can bring both states on resonance or change the time at which $\Delta(t) = 0$, by means of the dynamic Stark effect, provided that $\alpha_{11} \neq \alpha_{22}$. This is the idea behind the Stark shift chirped rapid adiabatic passage (SCRAP) scheme[116–119]. Notice that even though μ_{12} can be very weak, *e.g.* a transition between a bound state and a scattering or continuum state, by means of a strong pulse and by using an additional Stark effect (or a chirped pulse) one can in principle stimulate the transition and select the momentum of the continuum state. Conversely, even when $\Delta(t) = 0$ one can avoid the crossing at the unwanted time by means of a suitable Stark shifting. In the context of molecular processes this will be related to the creation of a light-induced avoided crossing (LIAC) or a light-induced conical intersection (LICI)[105–111]. This is also the idea behind the nonresonant dynamic Stark effect (NRDSE) scheme.

In the second case we take on a large μ_{12}, such that the effect of the laser on the system (goven by the Rabi frequency) is very strong. Typically in this case one neglects the Stark shift as its effect is much smaller than the changes induced by the direct coupling, which is responsible for Autler-Townes splittings. The dynamics can be described more easily in the adiabatic or dressed-state representation, which is carried by the instantaneous eigenstates of the time-dependent Hamiltonian, $\mathsf{H}\varphi_j(t) = \varepsilon(t)\varphi_j(t)$. Then if the system starts on a single dressed state, it will remain on this state during all times with high probability. That is, in this representation the Hamilltonian can be simplified again to a Hamiltonian with just one populated state. However now the nature of this single state

is strongly perturbed by the average effect of the remaining states. For relatively large $\Delta > \Omega$, the ratio of the populations P_j is [120,121]

$$\chi = \frac{P_2}{P_1} \sim \left(\frac{\Omega}{2\Delta}\right)^2 \tag{7}$$

However, if $\Delta(t)$ crosses the resonance ($\Delta = 0$), the changes are more dramatic: there is population inversion and the dressed state character will shift from resembling ϕ_1 to resembling ϕ_2. This is the essence of adiabatic rapid passage (ARP). [15,16]

2.2 Light-induced potentials

The full Hamiltonian of a molecule is rather complex. Although in this review we summarize results obtained in polyatomic molecules, as a first approach to qualitatively understanding the main theoretical concepts involved it is only necessary to consider what happens in diatomic molecules in the Born-Oppenheimer approximation and using the Floquet representation. Here and in the following this Floquet representation may refer to just the simplest RWA where the excited potential is shifted by the energy of a single photon.

A general Hamiltonian of the form

$$\mathbf{H} = \begin{pmatrix} \mathsf{T} & \mathsf{K} \\ \mathsf{K} & \mathsf{T} \end{pmatrix} + \begin{pmatrix} V_1(R) - \frac{1}{4}\alpha_{11}(R)\mathscr{E}^2(t) & -\frac{1}{2}\mu_{12}(R)\mathscr{E}(t) \\ -\frac{1}{2}\mu_{12}(R)\mathscr{E}(t) & V_2(R) - \hbar\omega - \frac{1}{4}\alpha_{22}(R)\mathscr{E}^2(t) \end{pmatrix} \tag{8}$$

where T is the kinetic energy, K takes into account non-adiabatic couplings and $V_j(R)$ are the electronic potential energy curves, can typically describe the most important phenomena occurring in the dynamics under a single strong field. [122] We have assumed that the field may be resonant or near-resonant between two electronic states, and nonresonant with respect to the remaining states of the molecule, although the one- and two-photon interactions could be due to different pulses.

Leaving aside the kinetic terms that let the nuclear wave function or wave packet move and spread and thus visit different regions of the potentials, the main difference between Eq. (5) and Eq. (8) is the fact that the detuning between the two states in the absence of an external field, $\Delta(R) = V_2(R) - V_1(R)$, changes for every value of the internuclear separation R. When $\Delta(R)$ is zero or very small at some bond lengths the dynamic polarizability is a strongly varying function of R. In this case again it is usually sufficient to consider just two electronic states.

We can again consider two cases, depending on the intensity of the coupling, $\mu_{12}\mathscr{E}$. When the coupling is weak, the laser induces a crossing between V_1 and V_2 whenever

$$\Delta(R,t) = V_2(R) - V_1(R) - \hbar\omega(t) - \frac{1}{4}\left(\alpha_{22}(R) - \alpha_{11}(R)\right)\mathscr{E}^2(t) = 0 \tag{9}$$

This coupling is usually termed a LIAC or, considering the vectorial nature of the coupling (as explained below) a LICI. Through the LICI, the nuclear wave packet can transfer part of the population. It operates in analogous way to a molecular (beyond Born-Oppenheimer-like) internal conversion, induced by K. This is typically the case when two weakly-coupled states are connected by the laser, *e.g.* when the Franck-Condon factor for the transition is very small.

On the other hand, when the coupling is strong (either because of μ_{ij} or because the field is very intense), similarly to what we described for the strong quasi-resonant coupling in the previous section, it is usually simpler to describe the system using dressed potentials or LIPs, in terms of which the potential energy matrix operator (including the coupling with the field) is diagonal. Considering only the most important effects, in this dressed state (DS) representation the Hamiltonian is diagonal,

$$\mathbf{H}^{\mathrm{DS}} \approx \begin{pmatrix} \mathsf{T} & 0 \\ 0 & \mathsf{T} \end{pmatrix} + \begin{pmatrix} V_1^{LIP}(R;\mathscr{E}) & 0 \\ 0 & V_2^{LIP}(R;\mathscr{E}) \end{pmatrix} \tag{10}$$

so the dynamics mainly occurs on a single LIP, V_1^{LIP}. But to characterize the LIP we need to know the structure of the strongly coupled electronic potentials, V_1 and V_2, as the electronic character of V_1^{LIP} completely changes due to the LIAC of the potentials in the Floquet representation,

$$V_1^{LIP}(R,\mathscr{E}) = \cos\theta(R,\mathscr{E})V_1(R) + \sin\theta(R,\mathscr{E})V_2(R) \tag{11}$$

where the mixing angle θ (obtained from diagonalizing the matrix of the potential energy including the field) changes from 0 to $\pi/2$ at both sides of the avoided crossing, R_c. In general, defining $\mathbf{U_{da}}$, the rotation matrix that diagonalizes the potential energy matrix ($\mathsf{H}^{\mathrm{DS}} = \mathbf{U}_{da}^{-1}\mathsf{H}\mathbf{U}_{da}$), the most important effect that may break the adiabatic dynamics implied by the Hamiltonian in Eq. (10) is given by the non-adiabatic coupling operator

$$\mathbf{H}_{\mathrm{NAC}}^{\mathrm{DS}} = -i\mathbf{U}_{da}^{-1}\frac{\partial}{\partial t}\mathbf{U}_{da} \tag{12}$$

which is large when the field $\mathscr{E}(t)$ changes fast enough that its derivative is large and the coupling [Eq. (12)] is of the or-

der of the energy gap between the LIPs. The first important effect that such an avoided crossing has in the LIPs is to completely deform the molecular potential energy curves and thus to change the structure of the molecule. For $V_1^{LIP}(R)$ the LIP looks like $V_1(R<R_c)$ before the crossing and like $V_2(R>R_c)$ after it.

Two typical cases are shown in Fig. 1. In the first one, two bound electronic states with displaced equilibrium geometries are resonantly coupled by the strong field. The ground LIP has a double-well structure, but for very strong field amplitudes it is possible to remove the barrier between the two wells or to permit tunneling near the barrier, thus allowing the wave function to move from the ground equilibrium geometry to the excited equilibrium configuration. On the other hand, in the excited LIP it is possible to induce adiabatic squeezing of the wave function.[78] In the second case, a bound potential is coupled to a dissociative electronic state. As observed in the figure, the coupling induces bond softening in the ground LIP (the dissociation energy is smaller) and bond hardening in the excited LIP, by which this potential bears some bound vibrational states. Since the position of the crossing, $V_1(R_c) = V_2(R_c) - \hbar\omega$, is controlled by the field, by exciting the system to V_2^{LIP} it is possible to stabilize the molecule at very large bond distances. This is the essence of all the laser adiabatic manipulation of the bond (LAMB) mechanisms.

In the previous cases the theoretical treatment of the dynamics implied mainly to consider what happened between two resonant or near resonant electronic states in the Floquet representation. When the detuning between the ground or initial state and the remaining states is very large, one should use polarizabilities. In many situations, when $\omega \ll V_j(R) - V_1(R)\ \forall j$ (at least in the regions visited by the nuclear wave packet) the static polarizability can be used. Since in the static polarizability the only spatial dependence comes from the transient dipole $\mu_{ij}(R)$, and it can often be neglected, the dynamics in this case lead to small spatial deformation. The main control in this scheme can be introduced by the time-dependence of the field and in many situations, the effective one electronic state problem can be qualitatively described by the effective one-level Hamiltonian of Eq. (2).

Before we proceed to describe specific control examples, we will briefly address the vectorial properties of the coupling. In Eq. (2) and all the following discussion, we have neglected the vectorial properties of the interaction. As indicated, in the Coulomb gauge the dipole (direct or one-photon) coupling is $\vec{\mu}_{12}\cdot\vec{E}^t(t) = \mu_{12}E(t)\cos\vartheta$, where ϑ is the angle between the laboratory-fixed polarization of the electric field and the molecular-fixed transient dipole moment. The coupling therefore depends on the orientation of the molecular axis with respect to the field. This explains why in a randomly aligned ensemble, even when the pulse is strong, there can be molecules (for $\vartheta = \pi/2$) that do not experience the coupling. This is also the reason that in diatomic molecules there can be LICIs.

On the other hand, the two-photon polarizability-mediated interaction is of the form $\vec{E}(t)\alpha_{jj}\vec{E}(t)$, where α_{jj} is a rank-two tensor. In diatomic molecules, defining z as the polarization vector (in the laboratory-frame coordinates), the interaction can be written as

$$V_{\rm int} = -\frac{1}{4}\left[\alpha_\perp + \cos^2\vartheta\left(\alpha_\parallel - \alpha_\perp\right)\right]\mathscr{E}^2(t) \qquad (13)$$

where $\alpha_\parallel$ and $\alpha_\perp$ are the polarizability components parallel or perpendicular to the molecular axis, respectively. Analogous expressions can be obtained for any other choice of laser polarization. The interaction given in Eq. (13) defines a torque that induces alignment of the molecules with respect to the field. That is, the polarization makes the molecular dipole to orient with respect to the external field. This can be regarded as the first application of control via polarization, where depending on the dynamics induced by $\mathscr{E}(t)$ (adiabatic, sudden or mixtures of the above) very interesting effects can be observed, as described in detail in several review articles.[57,98–100]

3 Demonstrations of strong laser field control of photochemistry

3.1 Strong field control of the absorption spectrum

Because of the reflection principle[123], under very general approximations[124] the absorption spectrum obtained from an electronic state j after excitation with an ultrashort pump pulse of carrier frequency ω_p and bandwidth $\Delta\omega_p$ in the absence of competing channels, is proportional to

$$P_j(\omega_p) \sim \exp\left[-\left(\frac{D_{j1}-\hbar\omega_p}{\hbar\Delta\omega_p}\right)^2\right] \qquad (14)$$

where $D_{j1} = V_j(R) - V_1(R)$ is the potential energy gap at the Franck-Condon (FC) region. Equation (14) only shows that the excitation probability quickly decays when the pulse is out of resonance. However, using a strong nonresonant field $\mathscr{E}_S$ in addition to the pump pulse, the electronic states are Stark-shifted. The same level of theory leads to a similar expression where instead of D_{j1} one needs to use the Stark-shifted energy gap[120]

$$D^p_{j1}(\mathscr{E}_S) = V_j^p(R) - V_1^p(R) \approx D_{j1} - \frac{1}{4}\left(\alpha_{jj}-\alpha_{11}\right)\mathscr{E}_S^2 \qquad (15)$$

The position of the absorption bands corresponding to different electronic channels can therefore be controlled[120]. The control can be more effective when the polarizabilities α_{jj} have different signs for different electronic states, such that

$\mathscr{E}_S$ can both blue-shift and red-shift the different bands of the spectrum.

An experimental demonstration of Stark control on the second absorption *B*-band of CH_3I at around 200 nm in terms of spectral shifts in the absorption lines has been recently reported[125,126]. In this wavelength region, absorption is dominated by transitions to the 6*s* member of a molecular Rydberg series and, in particular, to the optically active $^3R_1$ state (see Figure 2a).[127] These Rydberg orbitals are bound in character and the spectrum in this zone shows discrete transitions to the different vibrational levels[128], which are shown in Figure 2b. The absorption lines are lifetime broadened due to electronic predissociation in a time scale of the order of the picosecond induced by the coupling of the $^3R_1$ state with strongly repulsive members of the first absorption *A*-band, the most relevant being the $^3A_1$ state (see Figure 2a).[127] This electronic predissociation yields CH_3 fragments with some degree of vibrational excitation in the C–H stretch (ν_1) and umbrella (ν_2) modes in coincidence with spin-orbit excited $I^*(^2P_{1/2})$ atoms.

In these experiments, a single-photon transition to the vibrationless level of the Rydberg state (0_0^0 transition) of CH_3I was promoted with a femtosecond laser pump pulse centered at 201.2 nm. The Abel-inverted velocity map image of the CH_3 fragment (see ref.[125] for details of the experimental method), obtained after a (2+1) REMPI process induced with a sufficiently delayed 333.5 nm pulse, can be seen in Figure 2c. It contains two rings corresponding to contributions that can be assigned to the formation of spin-orbit excited $I^*(^2P_{1/2})$ and either $CH_3(\nu$=0) or $CH_3(\nu_1$=1). Other vibrationally excited CH_3 products can be detected by tuning the REMPI laser to the desired resonances.[129]

The rings present in the CH_3 image obtained in the conditions described above vanish entirely when a moderately intense near infrared (NIR) control laser pulse (around 5 TW cm^{-2}) is added in temporal overlap with the 201.2 nm pump pulse.[125,126] This can be seen in Figure 3a, where a map of the kinetic energy distribution of the CH_3 fragment as a function of pump-control delay is depicted. In this case, the NIR pulse centered at 800 nm was around 4 ps full-width-half-maximum (FWHM), and caused *B*–band absorption suppression during a temporal interval of almost 10 ps. The clearest evidence that absorption suppression is caused by a Stark shift effect lies in the recovery of the *B*-band characteristic signal upon frequency retuning of the pump pulse wavelength towards the blue. This is shown in the map depicted in Figure 3b, which is equivalent to that of Figure 3a, but which was acquired with a pump pulse tuned by 0.7 nm (20 meV) to the blue with respect to the NIR field-free condition. It can be seen that the region of temporal overlap between the strong NIR pulse and the pump pulse produced *B*–band signal enhancement in this case. The appearance of new contributions in the kinetic energy distribution maps will be described and explained in Section 3.3.4.

The results presented above allow to calibrate the strength of the Stark shift in the 0_0^0 transition peak of the *B*–band in CH_3I caused by the intense NIR field. This was done by retuning the pump laser wavelength in the presence of the NIR control field until the optimized *B*–band signal was recovered at different NIR field intensities. Figure 4 shows the Stark shift that was observed as a function of the NIR laser intensity.[125,126] The figure shows a linear dependence of the Stark shift with control laser intensity, as is expected for a second-order process[64]. In order to rationalize these findings, a numerical simulation was performed where Stark-shifted spectra were obtained by Fourier transform of the autocorrelation function obtained by propagating a nuclear wave packet in the Franck-Condon region of the *B* state, in the presence of a constant 800 nm field of different intensities. This strong nonresonant control field induces Stark-shift by coupling the initial *B* state to the *X* and whatever states. The potential energy curves, dipole couplings and spin-orbit couplings were obtained in a single dimension (corresponding to the C–I distance) by *ab initio* calculations at the multi reference configuration interaction (MRCI) level and using the AMFI approximation for the calculation of the spin-orbit coupling.[126] The simulation, as well as the experiment, found a blue shift of the transition line, but the magnitude of the Stark shift strength is underestimated in the simulation, possibly due to the reduced number of electronic states that were considered in the calculation as candidates to couple with the *B* state, and/or the fact that multiple-photon quasi-resonances were neglected.

3.2 Strong field control of state lifetimes

Several interesting schemes have been proposed to manipulate the lifetimes of predissociative states that use quantum interfering processes.[130–137] Quantum control with strong pulses via Stark effect can be used as well. Consider, in the simplest case, a predissociative coupling between a vibrational state in a bound potential $\phi_{i,v}$, and a continuum state in a dissociative potential $\phi_{f,E}$ that, following the Fermi golden rule, depends on the overlap between the nuclear wave functions and the density of continuum states $\rho(E)$ at the given energy,

$$\Gamma_v = \frac{2\pi}{\hbar}\left|\langle\phi_{i,v}|\phi_{f,E}\rangle\right|^2\rho(E)\delta(E-E_v) \qquad (16)$$

Clearly, Γ_v can be controlled by Stark-shifting the spectra:

$$E'-E_v \xrightarrow{\mathscr{E}} E' = E - \frac{1}{4}\left(\alpha_{i,v}-\alpha_{f,E}\right)\mathscr{E}^2 - E_v \qquad (17)$$

Then, if we want to increase the predissociation time we need to choose $\mathscr{E}$ such that either $\rho(E') \ll \rho(E)$ or the Franck-Condon factor $\langle\phi_{i,v}|\phi_{f,E'}\rangle$ is much smaller than $\langle\phi_{i,v}|\phi_{f,E}\rangle$. To decrease the lifetime we need to find $\mathscr{E}$ to do the opposite effect. Sometimes, using quasi-resonant processes, the crossing

between bound states and dissociative states can induce predissociation (or the opposite effect) in a more effective way.

An experimental demonstration of significant lifetime modification of the first accesible Rydberg state in CH_3I (the $^3R_1$ state constituting the *B*–band) was recently reported[125]. As mentioned above, the vibrational levels of this state are lifetime broadened due to electronic predissociation caused by the coupling with members of the strongly repulsive *A*–band (Figure 2a). This interaction causes electronic predissociation in times of the order of the picosecond. In Figure 3, we showed how the presence of a NIR field during the excitation and predissociation processes opens up two new channels that will be described in detail in Section 3.3.4. These new channels can be regarded as additional couplings of the initial state, and this is expected to cause a reduction of the state lifetime. A measurement of the lifetime in the presence of the NIR field was performed by recording CH_3 fragment images as a function of the time delay between the pump pulse (resonant with the 0_0^0 transition of the *B*–band) and the probe pulse (causing 2+1 REMPI in the CH_3 fragment), in conditions where a long (4 ps) NIR field of a range of intensities was applied in temporal coincidence with the pump pulse.

Figure 5 shows the result of integrating the section of the CH_3 image that corresponds to the *B*-band predissociative process (outer rings in Figure 2c) as a function of the pump-probe time delay. This was done in field-free conditions (panel (a)) and for a range of intensity values of the NIR control pulse from 0.18 TW cm^{-2} up to 0.55 TW cm^{-2}. The rise in the CH_3 transient follows a single exponential with a time constant that is equal to the lifetime of the precursor molecular Rydberg state in the presence of the field. It can be seen that the field-free value of the lifetime (1.5 ps) is reduced to less than half of its original value for the highest fields applied, with a measurement as low as 650 fs (panel (d)).

3.3 Strong field control of quantum yields

3.3.1 Control of photodissociation by nonresonant dynamic Stark effect. When two excited states V_1 and V_2 are degenerate or nearly degenerate in a region of the coordinate space, there can be nonadiabatic couplings between the states. The corresponding photochemical process around a nonadiabatic crossing can be controlled dynamically by means of a nonresonant control pulse $\mathscr{E}_S(t)$, depending on how close or how far is the crossing from the Franck-Condon window. This is the scenario where the dynamic Stark control methodology was originally proposed and its effects tested experimentally.

The first experimental demonstration of nonresonant dynamic Stark control of quantum yields in a photodissociation reaction was reported in 2006 by Stolow and coworkers[102]. A considerable degree of control was proven on the branching ratio of the dissociation of the diatomic IBr molecule. The situation is schematically shown in Figure 6a. From the IBr ground state ($X\ ^1\Sigma^+_{0^+}$), absorption in the visible takes place to the bright $A\ ^3\Pi_{0^+}$ state (*B* state in the Figure). Along the dissociation coordinate, the wave packet encounters a nonadiabatic intersection between states $A\ ^3\Pi_{0^+}$ and $B\ ^3\Sigma^-_{0^+}$ (*Y* state in the Figure) that lead to the distinct neutral atomic channels I+Br($^2P_{3/2}$) and I+Br*($^2P_{1/2}$) with a natural branching ratio of [Br*]/[Br]=3.5. The control method implied the application of an ultrashort nonresonant IR pulse (the control pulse) centered at 1.7 μm of nonperturbative intensity but below the onset for ionization. This pulse modified the potential energy curves via the Stark effect, and this had final consequences on the branching ratio if it was applied in one of two critical moments in the dissociation process, as can be seen in the velocity distribution map of Figure 6b.

The first critical moment is the initiation of the process, that is, near temporal overlap between the pump and control pulses. If the absorption step takes place in Stark-modified potential energy curves, this causes a change in the available energy, and the velocity of the dissociating wave packet changes, leading to a lower probability of surface hopping to the $B\ ^3\Sigma^-_{0^+}$ state and consequently a severely reduced [Br*]/[Br] ratio. The other critical time for the application of the control pulse is at a time delay where the wave packet reaches the crossing region, which happens around 300 fs after excitation. In that case, the effect was attributed to laser-induced changes of the adiabatic barrier, which enhance the probability for crossing, and thus cause a higher [Br*]/[Br] ratio.

In later theoretical work, Worth and coworkers[138] were able to demonstrate control of the products branching ratio in the photodissociation of IBr by changing the topography of the potential energy curves in the region of the nonadiabatic coupling. Using a three-state model, varying the parameters of the model and comparing to the simulated wave packet dynamics, they identified two different control mechanisms available in the two-pulse NRDSE experiment. A first control mechanism, that occurs when the pump and control pulses overlap in time, is due to the Stark effect induced by the control pulse, which shifts up the $A\ ^3\Pi_{0^+}$ state relative to the ground state. The second mechanism acts when the wave packet has reached the center of the avoided crossing and is due to changing the barrier height on the adiabatic curve. The major effect is due to the Stark shift upwards of the *A* state relative to the *B* state, which moves the avoided crossing to shorter distances. Thus, the wave packet reaches the crossing earlier, staying longer on its evolution and increasing the amount of crossing, which produces a decreasing of the branching ratio. At longer times, the crossing is left behind the evolving wave packet, so the the amount of crossing decreases and the branching ratio increases. The main disagreement between these theoretical predictions and the experiment is the timescale at which the positive and negative [Br*]/[Br] branching ratio is observed.

3.3.2 Control of photoisomerization yields. A newly demonstrated method for the control of a photoinduced process relies in the use of LICIs [105–111].

The creation of a LICI can be regarded as a resonant dynamic Stark effect; that is, it relies on resonant couplings between field-free states. Bucksbaum and coworkers recently reported the first experimental evidence for the creation of a LICI that plays an important role on the control of a photoisomerization reaction [112]. The authors explore the process of ring opening in 1,3-cyclohexadiene (CHD), which leads with about 50% probability to isomerization into 1,3,5-hexatriene (HT) on the ground electronic state in the absence of any external strong field.

After excitation in the UV, absorption takes place to a bright $1B$ state that rapidly crosses to the $2A$ state (S_1 in the Figure) through a conical intersection. There, the wave packet evolves until it finds a conical intersection with the ground $1A$ state (S_0 in the Figure), which is depicted with a red circle in Figure 7a. In this position of the potential energy surface, the geometry is very close to the transition state geometry for isomerization and, as a consequence, the wave packet can branch with almost equal probability either back to the recovery of the CHD reactant, or towards the formation of its HT isomer.

This region is thus particularly sensitive to perturbations, as it has been proven by the authors by adding an intense IR laser field at 800 nm, which caused a pronounced decrease in isomerization probability (see Figure 7b). It is best to consider the mechanism of laser control in this case by using a dressed state Born-Oppenheimer basis (Floquet picture), where the dressed states have energies shifted from those of the unperturbed states by integer multiples of the photon energy. New, laser induced, conical intersections appear, as indicated with blue circles in Figure 7a, and when the wave packet crosses back to the ground state through this LICI, it does so in a region where the geometry is distant from the transition state isomerization geometry, and therefore it recovers the original CHD form. Therefore, photoisomerization is notably reduced when an intense NIR laser pulse is present.

3.3.3 Control of direct photodissociation in a polyatomic molecule. Recently, we have reported an experimental demonstration where the creation of a LICI is exploited to control the branching ratio of a two-channel direct photodissociation reaction in a polyatomic molecule. [113] The scheme is shown in Figure 8 and has analogies with the work of Bucksbaum *et al.* [112] in that the creation of a LICI causes a certain probability of return to the ground electronic state before the wave packet significantly evolves on the excited state where it is originally born, and this causes a change in the final products of the reaction.

The process under study was *A*–band rapid dissociation in CH_3I induced by ultrashort pump pulses at 268 nm. The experiment involved the observation of the CH_3 product from dissociation of CH_3I in the presence of a moderately intense (5 TW cm^{-2}) and relatively long (4 ps) NIR (804 nm) pulse. The resulting CH_3 fragments were ionized through a (2+1) REMPI process at 333.5 nm and its velocity vector and angular distributions were analyzed by velocity map imaging where images were acquired for a set of pump-control delays. Three of those images are shown in Figure 9a. The bottom image was acquired at a delay where the control pulse preceded the pump pulse, and is identical to that registered in field-free conditions [139,140] . It shows the well known I($^2P_{3/2}$) and I*($^2P_{1/2}$) channels (outer and inner anisotropic rings, respectively). For the middle and top images, the control pulse was present during the excitation and dissociation process, and a new contribution appears on the images as a new ring with significantly lower kinetic energy. This contribution can be clearly seen in the CH_3 kinetic energy distribution maps depicted in Figure 9b as a tilted contribution at around 0.6 eV of center-of-mass CH_3 kinetic energy.

A simplified one-dimensional (1D) model in the dressed-state picture using a Floquet representation has been shown to be sufficient to describe the main mechanism of the control exerted by the moderately intense and relatively long NIR pulse on this photodissociation reaction. Figure 10 shows the temporal evolution of the photodissociating wave packet in momentum space for three different control pulse situations, in a time window from few femtoseconds before the application of the pump pulse and until the wave packet reaches the asymptotic limit. This picture provides the transient kinetic energy distributions of the fragments. Without the control pulse (see Figure 10a), the dynamics occurs on the unperturbed potential energy surfaces. In the first tens of femtoseconds the wave packet rapidly gains a large momentum on the $^3Q_0$ (V_e) potential energy surface (this is not apparent in the figure due to contrast). Immediately afterwards, the kinetic energy of the excited wave packet is slightly reduced because the potential has a shallow well, and then the molecule dissociates directly, reaching the asymptotic state in approximately 100 fs. It should be noted that in the complete description, after the pump pulse creates a wave packet in the repulsive $^3Q_0$ state, it evolves towards dissociation and very soon encounters a natural conical intersection with the $^1Q_1$ surface (see Figure 8), where some population transfer occurs, leading to part of the wave packet ending in the minor I($^2P_{3/2}$) channel, but most remaining in $^3Q_0$, which correlates with the major I*($^2P_{1/2}$) channel. However, the simplified 1D model only considers the $^3Q_0$ and ground electronic potential energy surfaces for simplicity and cannot account for the minor I($^2P_{3/2}$) channel caused by the $^3Q_0/^1Q_1$ conical intersection.

With a relatively weak (5 TW cm^{-2}) and long (3.9 ps FWHM) control pulse that temporally overlaps with the pump pulse and continues on until the wave packet reaches the

asymptotic state (Figure 10b), part of the wave packet crosses through the LICI and dissociates in the ground electronic state. In this case, the asymptotic kinetic energy distribution in the ground state mimics that on the excited state, but is shifted to the red in momentum space due to the attractive nature of this potential for long internuclear distances. This corresponds to the observations shown in Figure 9. The emergence of this new process causes a decrease in the $[I^*]/[I]$ ratio, since the part of the wave packet now dissociates on the ground electronic state, which correlates with ground state $I(^2P_{3/2})$ atoms.

It is interesting to note that for higher intensities (around 80 TW cm^{-2}) and relatively long (3.9 ps) fields, such as those used for the simulation depicted in Figure 10c, the dynamics basically occurs on the LIPs. The relation between LIPs and field-free molecular potentials is schematically depicted in the Figure and also in Figure 8. The excited LIP, hereafter V_e^a, correlates to the field-free V_e before the crossing C−I distance, R_c, and to the ground electronic state (hereafter V_g) after R_c. The ground LIP, hereafter V_g^a, correlates to V_g before and to V_e after R_c. Both LIPs show a smooth curvature around the LICI. In this representation, the wave packet excited on V_e moves coherently on a single LIP, V_e^a, and feels the attractive section of this LIP, thus suffering a decrease in kinetic energy. Since the laser field is always on while the wave packet evolves around the region of the avoided crossing, the only component that survives asymptotically when the transition dipole moment decays is the ground state, V_g. It is remarkable that, in this case, a complete asymptotic wave packet transfer to the ground state is achieved. Therefore, in these conditions it is possible to bring the I^* quantum yield to almost zero, since dissociation at these high intensities of the control field would proceed entirely on the LIP that correlates asymptotically with $I(^2P_{3/2})$ atoms. No experimental equivalent of this situation could be tested on this system, due to the high laser intensity that needs to be sustained for a long time.

3.3.4 Control of electronic predissociation. A related phenomenon was observed recently in the slower, predissociation-mediated bond fission of CH_3I in the *B*–band[125] . In Section 3.1 we described how a strong NIR field (804 nm) Stark-shifted the discrete resonances of the *B*–band and how upon pump laser wavelength retuning the CH_3 images contained not only the *B*–band characteristic rings, but also two additional contributions. This can be seen in Figure 11. The CH_3 images were acquired using a 201.2 nm pump pulse for 0_0^0 transition *B*–band excitation and a 333.5 probe beam for CH_3 (2+1) resonant multiphoton ionization process. The image in Figure 11a was acquired in field-free conditions, while that in Figure 11b was acquired under a 804 nm, 4 ps FWHM field of moderate intensity (0.55 W cm^{-2}). One of the new contributions observed in the image in Figure 11b consists of an enhanced signal in the central part, *i. e.* CH_3 ions with low kinetic energy. This is attributed to multiphoton dissociative ionization processes that take place during the temporal overlap of the pump and NIR control pulses. The other new contribution is a well-defined ring with lower kinetic energy than those corresponding to *B*–band predissociation, parallel angular character and a kinetic energy that shifts as a function of the temporal delay between the pump pulse and the NIR control pulse, as was already shown above in Figure 3. This new channel has been attributed to a dump process, where the NIR pulse produces stimulated emission and transfer of population from the vibrationless level of the $^3R_1$ Rydberg state to the $^3Q_1$ dissociative valence state, as is schematically depicted in Figure 11c. Alternatively, this can be viewed as a laser-induced avoided crossing (LIAC), between two excited potential energy surfaces ($^3R_1$ and $^3Q_1$), the latter shifted by the photon energy. This dump process finally leads to rapid dissociation on the repulsive $^3Q_1$ potential energy surface, which correlates with CH_3+$I(^2P_{3/2})$. In these conditions, the quantum yield Φ^*, defined as $\Phi^*=[I^*]/([I]+[I^*])$, which is unity for *B*–band electronic predissociation from the ground vibrational state of the $^3R_1$ Rydberg state, is significantly reduced in the presence of the NIR field.

3.4 Control of fragment kinetic energy in direct photodissociation

An experimental demonstration of control over the kinetic energy distribution of fragments formed in the main channel of a direct photodissociation reaction of a polyatomic molecule using the scheme presented above was recently reported in Ref.[113]. In Section 3.3.3, we presented the changes induced by a relatively long NIR field of about 5 TW cm^{-2} in the photodissociation of CH_3I in the *A*–band. The main finding in those conditions was the appearance of a lower kinetic energy channel that results from the creation of a LICI between the excited and the ground state. In the description of those experiments, the temporal changes in kinetic energy, that were clear in Figure 9a, were not discussed. It is clear from the Figure that the new channel that corresponds to the passage through the LICI shows chirped behavior, *i.e.* its kinetic energy shifts as a function of the time delay between the pump and the control pulse. This is related to the inherent negative chirp of the control pulse: since the resonance condition for the creation of a LICI is met at earlier or later times as a function of the instantaneous frequency of the control pulse, the position of the LICI as a function of the bond distance changes in time. When the pump pulse is applied in the trailing edge of the control pulse, the instantaneous frequency is lower, and this causes the LICI to appear at large bond distances. In these conditions, the fragment kinetic energy acquired on the excited state is higher, and the barrier it has to overcome to dissociation is lower, which causes a blue shift in the final kinetic energy. The case is the

opposite when the pump pulse is applied in the leading edge of the control pulse, with a red shift of the kinetic energy. In this case, the chirp (or rather, the instantaneous frequency) of the control pulse acts as the knob that allows control of the kinetic energy of the LICI-mediated channel.

However, the use of shorter and more intense laser pulses greatly enriches the control possibilities over the kinetic energy of the fragments, since rapidly changing intensities cause fast switches between the dressed and the field-free states. When these are exerted during the wave packet evolution in the proximity of the LICI, the adiabaticity is broken and the dynamics can be modified to a greater extent. In the next we will show how it is possible to produce changes in the kinetic energy of fragment produced in the the main channel of the direct photodissociation of CH_3I in the *A*-band through the application of this strategy.

The experiment is a modification of that already described in Section 3.3.3, where *A*-band photodissociation of CH_3I is initiated with UV pump pulses at 268 nm and the CH_3 fragments are later probed by through a REMPI process at 333.5 nm and the ions detected in velocity map configuration. In this case, the long NIR control pulse used in Section 3.3.3 is replaced by a short (50 fs) and more intense (80 TW cm^{-2}) pulse. Figure 12 shows the kinetic energy distribution of $CH_3(v{=}0)$ as a function of pump-control time delay in these conditions.

The first observation from these results is that the LICI-mediated channel is still visible, albeit significantly broadened in kinetic energy and only present during a narrow temporal overlap. More interestingly, the main dissociation channel producing $I^*(^2P_{1/2})$ atoms is remarkably broadened, with a distribution clearly bent towards lower kinetic energies at time delays corresponding to the application of the control pulse during the initial stages of the wave packet evolution towards dissociation.

In this case, it has been essential to add another ingredient (beyond intensity and chirp) to achieve control on the kinetic energy distribution of fragments appearing through the main *A*–band dissociation channel. This ingredient has consisted of the application of a pump-control temporal sequence that exploits the presence of a resonance condition at a given internuclear distance to cause rapid switches between the dressed and field-free states during the propagation of the wave packet.

Figure 13 shows the application of the 1D model in the dressed-state picture (Floquet representation) described in Section 3.3 to the new situation. In the Figure, the time evolution of the photodissociating wave packet is shown for a selected time delay between the pump and control pulses of 60 fs. The FWHM of the pump pulse has been set at 50 fs and, depending on the momentum component, the wave packet takes from around 50 to 100 fs to reach the LICI (at R_c, see Section 3.3.3). The choice of a 60 fs time delay is motivated by the need to provoke rapid changes in the intensity of the control pulse during the transit of the wave packet through the LICI. In particular, it was observed that for a 60 fs time delay the fastest momentum components of the wave packet reach R_c before the control pulse acts, to naturally yield $I^*(^2P_{1/2})$. In contrast, the slowest momentum components cross R_c when the control pulse is at its maximum intensity, so they follow the LIP, dissociating in V_g and therefore yielding ground state $I(^2P_{3/2})$. Under these conditions, the pulse sequence acts as a momentum filter that discriminates the velocity components of the dissociating wave packet on the different reaction channels.

The energy distribution filtering (narrowing of the KED) is not the sole effect of the application of these short control pulses. As is clear from the experimental Figure 12, and also in the velocity distribution of Figure 13, there is a significant red shif of the KEDE in the main dissociation channel. This is a typical signature of non-adiabatic effects. Indeed, as the crossing is created, there is an abrupt ramp up from a low to a high control field intensity, and thus the wave packet initially evolving on V_e is mainly transferred to the V_g^a LIP, but as its shape is attractive, as opposed to repulsive, this reduces the momentum of the dissociating wave packet as it evolves, causing the red shift of the KEDE that is evident both in the simulation and in the experimental result of Figure 12. Of course the transfer from V_e to V_g^a is not complete, and there is a low probability to appear on the other LIP, V_e^a, which correlates with the ground state V_g after R_c, and this appears as the lower energy, LICI-mediated channel apparent again both in the simulation and as the minor contribution in the experimental Figure 12. These results show that a timely breakdown of the adiabaticity is an essential tool to manipulate the kinetic energy distributions, and that it is possible to access this regime simply by controlling the time delay between the pump and control pulses of the required time duration, typically in the femtosecond scale.

4 Conclusions

This Perspective has sought to summarize recent achievements in strong laser control of photochemical processes, while providing a theoretical framework that describes the new phenomena that underlie the control mechanisms. It seems evident that the strong, and highly controllable electromagnetic fields provided by state-of-the-art ultrafast lasers are appropriate tools to control nuclear and electron dynamics at the microscopic level, but there is still a long route to achieve high yields in the desired channels, to reduce unwanted channels induced by the lasers and to devise new schemes of control that can address the varied problems that appear in photochemistry. Constant connection between theory and experiment is in our view essential to direct the efforts towards

realizable schemes. The combination of strong laser fields that dress the intramolecular interactions and ultrashort, attosecond pulses that can freeze electron dynamics is bound to greatly increase our understanding of molecular dynamics in the presence of light.

Acknowledgements

We acknowledge the contributions to the work presented in this paper by M. E. Corrales, G. Balerdi, Dr. G. Gitzinger, Dr. V. Loriot and Dr. B. Y. Chang. This work has been financed by the Spanish MICINN and MINECO through Grants No. CTQ2012-36184, CTQ2012-37404-C02-01, the Consolider program Science and Applications of Ultrafast Ultraintense Lasers, Grant No. CSD2007-00013, and by the European Union ITN network Ultrafast control of quantum systems by strong laser fields-FASTQUAST (Grant No. PITN-GA-2008-214962). This research has been performed within the Unidad Asociada Química Física Molecular between Departamento de Química Física of UCM and CSIC. The facilities provided by the Centro de Láseres Ultrarrápidos (UCM) are gratefully acknowledged.

References

1 A. H. Zewail, *Physics Today*, 1980, **33**, 27.
2 J. J. Gerdy, M. Dantus, R. M. Bowman and A. H. Zewail, *Chem. Phys. Lett.*, 1990, **171**, 1.
3 E. D. Potter, J. L. Herek, P. S., Q. Liu and A. H. Zewail, *Nature*, 1992, **355**, 66.
4 P. Brumer and M. Shapiro, *Annu. Rev. Phys. Chem.*, 1992, **43**, 257.
5 R. J. Gordon and S. A. Rice, *Annu. Rev. Phys. Chem.*, 1997, **48**, 601.
6 H. Rabitz, R. de Vivie-Riedle and K. Kompa, *Science*, 2000, **288**, 824.
7 S. A. Rice and M. Zhao, *Optical Control of Molecular Dynamics*, Wiley-Interscience, 2000.
8 P. W. Brumer and M. Shapiro, *Principles of the Quantum Control of Molecular Processes*, Wiley-Interscience, 2003.
9 D. Goswami, *Phys. Rep.*, 2003, **374**, 385.
10 T. Brixner and G. Gerber, *ChemPhysChem*, 2003, **4**, 418.
11 G. Nuernberger, G. Vogt, T. Briner and G. Gerber, *Phys. Chem. Chem. Phys.*, 2007, **9**, 2470.
12 D. D'Alessandro, *Introduction to Quantum Control and Dynamics*, Chapman Hall and CRC Boca Raton FL, 2007.
13 G. G. Balint-kurti, S. Zou and A. Brown, *Adv. Chem. Phys.*, 2008, **138**, 43.
14 C. Brif, R. Chakrabarti and H. Rabitz, *Adv. Chem. Phys.*, 2012, **148**, 1.
15 K. Bergmann, H. Theuer and B. W. Shore, *Rev. Mod. Phys.*, 1998, **70**, 1003.
16 N. V. Vitanov, T. Halfmann, B. W. Shore and K. Bergmann, *Annu. Rev. Phys. Chem.*, 2001, **52**, 763.
17 M. Shapiro and P. Brumer, *Advances In Atomic, Molecular, and Optical Physics*, Academic Press, 2000, vol. Volume 42, p. 287.
18 J. Oreg, F. T. Hioe and J. H. Eberly, *Phys. Rev. A*, 1984, **29**, 690.
19 U. Gaubatz, P. Rudecki, S. Schiemann and K. Bergmann, *J. Chem. Phys.*, 1990, **92**, 5363.
20 M. Shapiro and P. Brumer, *J. Chem. Phys.*, 1986, **84**, 4103.
21 D. J. Tannor, R. Kosloff and S. A. Rice, *J. Chem. Phys.*, 1986, **85**, 5805.
22 A. Peirce, M. Dahleh and H. Rabitz, *Phys. Rev. A*, 1988, **37**, 4950.
23 R. Kosloff, S. Rice, P. Gaspard, S. Tersigni and D. Tannor, *Chem. Phys.*, 1989, **139**, 201.
24 R. S. Judson and H. Rabitz, *Phys. Rev. Lett.*, 1992, **68**, 1500.
25 A. H. Zewail, *J. Phys. Chem. A*, 2000, **104**, 5660.
26 A. H. Zewail, *Science*, 1988, **242**, 1645.
27 M. J. Rosker, M. Dantus and A. H. Zewail, *J. Chem. Phys.*, 1988, **89**, 6113.
28 A. M. Weiner, J. P. Heritage and R. N. Thurston, *Opt. Lett.*, 1986, **11**, 153.
29 F. Spzno, M. Haner and W. Warren, *Chem. Phys. Lett.*, 1987, **135**, 97.
30 T. Brixner and G. Gerber, *Opt. Lett.*, 2001, **26**, 557.
31 M. Wollenhaupt, V. Engel and T. Baumert, *Annu. Rev. Phys. Chem.*, 2005, **56**, 25.
32 T. Brixner, T. Pfeifer, G. Gerber, M. Wollenhaupt and T. Baumert, *Femtosecond Laser Spectroscopy*, Springer-Verlag, New York, 2005, p. 225.
33 Y. Silberberg, *Annu. Rev. Phys. Chem.*, 2009, **60**, 277.
34 R. J. Levis, G. M. Menkir and H. Rabitz, *Science*, 2001, **292**, 709.
35 I. Pastirk, X. Zhu, V. V. Lozovoy and M. Dantus, *App. Opt.*, 2007, **46**, 4041.
36 V. V. Lozovoy, X. Zhu, T. C. Gunaratne, D. A. Harris, J. C. Shane and M. Dantus, *J. Phys. Chem. A*, 2008, **112**, 3789.
37 A. Assion, T. Baumert, J. Helbing, V. Seyfried and G. Gerber, *Chem. Phys. Lett.*, 1996, **259**, 488.
38 D. Irimia and M. H. M. Janssen, *J. Chem. Phys.*, 2010, **132**, 234302.
39 J. Ullrich, R. Moshammer, A. Dorn, R. Dörner, L. P. H. Schmidt and H. Schmidt-Böcking, *Rep. Prog. Phys.*, 2003, **66**, 1463.
40 A. Vredenborg, W. G. Roeterdink and M. H. M. Janssen, *Rev. Sci. Instrum.*, 2008, **79**, 063108.
41 A. Assion, T. Baumert, M. Bergt, T. Brixner, B. Kiefer, V. Seyfried, M. Strehle and G. Gerber, *Science*, 1998, **282**, 919.
42 C. Daniel, J. Full, L. González, C. Lupulescu, J. Manz, A. Merli, S. Vajda and L. Wöste, *Science*, 2003, **299**, 536.
43 T. Brixner, G. Krampert, T. Pfeifer, R. Selle, G. Gerber, M. Wollenhaupt, O. Graefe, C. Horn, D. Liese and T. Baumert, *Phys. Rev. Lett.*, 2004, **92**, 208301.
44 F. Vetter, M. Plewicki, A. Lindinger, A. Merli, S. Weber and L. Wöste, *Phys. Chem. Chem. Phys.*, 2005, **7**, 1151.
45 A. Lindinger, A. Merli, M. Plewicki, F. Vetter, S. Weber and L. Wöste, *Chem. Phys. Lett.*, 2005, **413**, 315.
46 B. Schaefer-Bung, V. Bonacic-Koutecky, F. Sauer, S. M. Weber, L. Wöste and A. Lindinger, *J. Chem. Phys.*, 2006, **125**, year.
47 P. Nuernberger, D. Wolpert, H. Weiss and G. Gerber, *Proc. Nat. Acad. Sci. USA*, 2010, **107**, 10366.
48 E. Wells, C. E. Rallis, M. Zohrabi, R. Siemering, B. Jochim, P. R. Andrews, U. Ablikim, B. Gaire, S. De, K. D. Carnes, B. Bergues, R. de Vivie-Riedle, M. F. Kling and I. Ben-Itzhak, *Nature Commun.*, 2013, **4**, 1.
49 T. Brixner, N. H. Damrauer, P. Niklaus and G. Gerber, *Nature*, 2001, **414**, 57.
50 J. L. Herek, W. Wohlleben, R. J. Cogdell, D. Zeidler and M. Motzkus, *Nature*, 2002, **417**, 533.
51 G. Vogt, G. Krampert, P. Niklaus, P. Nuernberger and G. Gerber, *Phys. Rev. Lett.*, 2005, **94**, 068305.
52 C. Trallero, B. J. Pearson, T. Weinacht, K. Gilliard and S. Matsika, *J. Chem. Phys.*, 2008, **128**, 124107.
53 J. Roslund and H. Rabitz, *Phys. Rev. A*, 2009, **80**, 013408.
54 K. W. Moore, A. Pechen, X.-J. Feng, J. Dominy, V. J. Beltrani and H. Rabitz, *Phys. Chem. Chem. Phys.*, 2011, **13**, 10048.
55 P. von den Hoff, S. Thallmair, M. Kowalewski, R. Siemering and R. de Vivie-Riedle, *Phys. Chem. Chem. Phys.*, 2012, **14**, 14460.
56 C. Brif, R. Chakrabarti and H. Rabitz, *Phys. Rev.*, 1955, **100**, 703.

57 D. Townsend, B. J. Sussman and A. Stolow, *J. Phys. Chem. A*, 2011, **115**, 357.
58 B. J. Sussman, *Am. J. Phys.*, 2011, **79**, 477.
59 A. Zavriyev, P. Bucksbaum, J. Squier and F. Saline, *Phys. Rev. Lett.*, 1993, **70**, 1077.
60 P. H. Bucksbaum, A. Zavriyev, H. G. Muller and D. W. Schumacher, *Phys. Rev. Lett.*, 1990, **64**, 1883.
61 J.-M. Yuan and T. F. George, *J. Chem. Phys.*, 1978, **68**, 3040.
62 A. D. Bandrauk, E. E. Aubanel and J.-M. Gauthier, *J.-M. Gauthier*, Dekker, New York, 1994.
63 B. M. Garraway and K.-A. Suominen, *Phys. Rev. Lett.*, 1998, **80**, 932.
64 B. Y. Chang, S. Shin, J. Santamaría and I. R. Solá, *J. Chem. Phys.*, 2009, **130**, 124320.
65 M. Rodriguez, K.-A. Suominen and B. Garraway, *Phys. Rev. A*, 2000, **62**, 053413.
66 I. R. Solá, J. Santamaría and V. S. Malinovsky, *Phys. Rev. A*, 2000, **61**, 043413.
67 I. Solá, B. Chang, J. Santamaría, V. Malinovsky and J. Krause, *Phys. Rev. Lett.*, 2000, **85**, 4241.
68 B. Y. Chang, I. R. Solá, J. Santamaría, V. S. Malinovsky and J. L. Krause, *J. Chem. Phys.*, 2001, **114**, 8820.
69 V. S. Malinovsky, J. Santamaría and I. R. Solá, *J. Phys. Chem. A*, 2003, **107**, 8259.
70 J. González-Vázquez, I. R. Solá and J. Santamaría, *J. Phys. Chem. A*, 2006, **110**, 1586.
71 J. Cao, C. Bardeen and K. Wilson, *Phys. Rev. Lett.*, 1998, **80**, 1406.
72 S. Kallush and Y. Band, *Phys. Rev. A*, 2000, **61**, 041401.
73 B. Chang, I. Solá, V. Malinovsky and J. Santamaría, *J. Chem. Phys.*, 2000, **113**, 4901.
74 M. Wollenhaupt, D. Liese, A. Präkelt, C. Sarpe-Tudoran and T. Baumert, *Chem. Phys. Lett.*, 2006, **419**, 184.
75 M. Wollenhaupt and T. Baumert, *J. Photochem. Photobiol., A*, 2006, **180**, 248.
76 T. Bayer, M. Wollenhaupt and T. Baumert, *J. Phys. B: At. Mol. Opt. Phys.*, 2008, **41**, 074007.
77 M. Wollenhaupt, T. Bayer, N. V. Vitanov and T. Baumert, *Phys. Rev. A*, 2010, **81**, 053422.
78 B. Y. Chang, S. Lee, I. R. Solá and Santamaría, *J. Chem. Phys.*, 2005, **122**, 204316.
79 B. Y. Chang, H. Rabitz and I. R. Solá, *Phys. Rev. A*, 2003, **68**, 031402.
80 I. R. Solá, B. Y. Chang and H. Rabitz, *J. Chem. Phys.*, 2003, **119**, 10653.
81 B. Y. Chang, S. Lee and I. R. Solá, *J. Chem. Phys.*, 2004, **121**, 11118.
82 B. Y. Chang, S. Shin and I. R. Solá, *Phys Rev. A*, 2010, **82**, 063414.
83 I. R. Solá, S. Shin and B. Y. Chang, *J. Chem. Phys.*, 2011, **134**, 104301.
84 B. Y. Chang, S. Shin, Santamaría and I. R. Solá, *J. Phys. Chem. A*, 2012, **116**, 2691.
85 B. Y. Chang, S. Shin, A. Palacios, F. Martín and I. R. Solá, *ChemPhysChem*, 2013, **14**, 1405.
86 B. Y. Chang, S. Shin, A. Palacios, F. Martín and I. R. Solá, *J. Chem. Phys.*, 2013, **139**, 084306.
87 J. González-Vázquez, I. R. Solá, J. Santamaría and V. S. Malinovsky, *J. Chem. Phys.*, 2006, **125**, 124315.
88 J. González-Vázquez, I. R. Solá, J. Santamaría and V. S. Malinovsky, *Chem. Phys. Lett.*, 2006, **431**, 231.
89 I. R. Solá, J. González-Vázquez and V. S. Malinovsky, *Phys. Rev. A*, 2006, **74**, 043418.
90 J. González-Vázquez, I. R. Solá, J. Santamaría and V. S. Malinovsky, *J. Phys. Chem. A*, 2007, **111**, 2670.
91 J. González-Vázquez, L. González, I. R. Solá and J. Santamaría, *J. Chem. Phys.*, 2009, **131**, 104302.
92 M. F. Kling, P. von den Hoff, I. Znakovskaya and R. de Vivie-Riedle, *Phys. Chem. Chem. Phys.*, 2013, **15**, 9448.
93 J. González-Vázquez, L. González, S. R. Nichols and T. C. Weinacht, *Phys. Chem. Chem. Phys.*, 2010, **12**, 14203.
94 D. Geissler, T. Rozgonyi, J. González-Vázquez, L. González, P. Marquetand and T. C. Weinacht, *Phys. Rev. A*, 2011, **84**, 053422.
95 D. Geissler, P. Marquetand, J. González-Vázquez, L. González, T. Rozgonyi and T. C. Weinacht, *J. Phys. Chem. A*, 2012, **116**, 11434.
96 P. Marquetand, T. Weinacht, T. Rozgonyi, J. González-Vázquez, D. Geissler and L. González, *Advances In Multi-photon Processes Spectroscopy*, World Scientific, 2013, vol. Vol. 21, p. 1.
97 P. Sándor, A. Zhao, T. Rozgonyi and T. C. Weinacht, *J. Phys. B*, 2014, **47**, 124021.
98 T. Seideman, *Rev. Mod. Phys.*, 2003, **75**, 543.
99 R. Torres, R. de Nalda and J. P. Marangos, *Phys. Rev. A*, 2005, **72**, 023420.
100 T. Seideman and E. Hamilton, *Adv. At. Mol. Opt. Phys.*, 2006, **52**, 289.
101 B. J. Sussman, M. Y. Ivanov and A. Stolow, *Phys. Rev. A*, 2005, **71**, 051401.
102 B. J. Sussman, D. Townsend, M. Y. Ivanov and A. Stolow, *Science*, 2006, **314**, 278.
103 B. J. Sussman, J. G. Underwood, R. Lausten, M. Y. Ivanov and A. Stolow, *Phys. Rev. A*, 2006, **73**, 053403.
104 P. J. Bustard, G. Wu, R. Lausten, D. Townsend, I. A. Walmsley, A. Stolow and B. J. Sussman, *Faraday Discuss.*, 2011, **153**, 321.
105 N. Moiseyev, M. Sindelka and L. S. Cederbaum, *J. Phys. B: At. Mol. Opt. Phys.*, 2008, **41**, 221001.
106 M. Sindelka, N. Moiseyev and L. S. Cederbaum, *J. Phys. B: At. Mol. Opt. Phys.*, 2011, **44**, 045603.
107 G. J. Halász, M. Sindelka, N. Moiseyev, L. S. Cederbaum and A. Vibók, *J. Phys. Chem. A*, 2011, **116**, 2636.
108 G. J. Halász, A. Vibók, M. Sindelka, N. Moiseyev and L. S. Cederbaum, *J. Phys. B: At. Mol. Opt. Phys.*, 2011, **44**, 175102.
109 G. J. Halász, A. Vibók, M. Sindelka, L. S. Cederbaum and N. Moiseyev, *Chem. Phys.*, 2012, **399**, 146.
110 A. Csehi, A. Bende, G. J. Halász, A. Vibók, A. Das, D. Mukhopadhyay, S. Mukherjee, S. Adhikari and M. Baer, *J. Phys. Chem. A*, 2013, **117**, 8497.
111 P. V. Demekhin and L. S. Cederbaum, *J. Chem. Phys.*, 2013, **139**, 154314.
112 J. Kim, H. Tao, J. L. White, V. S. Petrović, T. J. Martinez and P. H. Bucksbaum, *J. Phys. Chem. A*, 2012, **116**, 2758.
113 M. E. Corrales, J. González-Vázquez, G. Balerdi, I. R. Solá, R. de Nalda and L. Bañares, *Nature Chem.*, 2014, **6**, 785.
114 B. W. Shore, *Manipulating Quantum Structures Using Laser Pulses*, Cambridge University Press, Cambridge, UK ; New York, Edicion: New. edn, 2011.
115 P. R. Berman and V. S. Malinovsky, *Principles of Laser Spectroscopy and Quantum Optics*, Princeton University Press, 2010.
116 A. A. Rangelov, N. V. Vitanov, L. P. Yatsenko, B. W. Shore, T. Halfmann and K. Bergmann, *Phys. Rev. A*, 2005, **72**, 053403.
117 B. Chang, H. Choi, S. Shin and I. Sola, *Phys. Rev. A*, 2007, **75**, 063405.
118 B. Y. Chang and I. R. Sola, *Chem. Phys.*, 2007, **338**, 228.
119 M. Oberst, H. Münch and T. Halfmann, *Phys. Rev. Lett.*, 2007, **99**, 173001.
120 B. Y. Chang, S. Shin, J. Santamaría and I. R. Sola, *J. Chem. Phys.*, 2009, **130**, 124320.
121 B. Y. Chang, S. Shin and I. R. Solá, *J. Chem. Phys.*, 2009, **131**, 204314.
122 H. Rabitz, R.-B. Wu, T.-S. Ho, K. M. Tibbetts and X. Feng, *Recent Advances in the Theory and Application of Fitness Landscapes*, Springer Berlin Heidelberg, 2014, p. 33.
123 R. Schinke, *Photodissociation Dynamics: Spectroscopy and Fragmentation of Small Polyatomic Molecules*, Cambridge University Press, Cambridge England ; New York, Edicin: Revised edition edn, 1993.

124 S. Meyer, C. Meier and V. Engel, *J. Chem. Phys.*, 1998, **108**, 7631.

125 M. E. Corrales, G. Balerdi, V. Loriot, R. d. Nalda and L. Bañares, *Faraday Discuss.*, 2013, **163**, 447.

126 G. Balerdi, M. E. Corrales, G. Gitzinger, J. González-Vázquez, I. R. Solá, V. Loriot, R. de Nalda and L. Bañares, *EPJ Web of Conferences*, 2013, **41**, 02035.

127 A. B. Alekseyev, H.-P. Liebermann and R. J. Buenker, *J. Chem. Phys.*, 2011, **134**, 044303.

128 A. P. Baronavski and J. C. Owrutsky, *J. Chem. Phys.*, 1998, **108**, 3445.

129 G. Gitzinger, M. E. Corrales, V. Loriot, R. d. Nalda and L. Bañares, *J. Chem. Phys.*, 2012, **136**, 074303.

130 F. Chateauneuf, T. T. Nguyen-Dang, N. Ouellet and O. Atabek, *J. Chem. Phys.*, 1998, **108**, 3974.

131 E. Frishman and M. Shapiro, *Phys. Rev. Lett.*, 2001, **87**, 253001.

132 M. Sukharev and T. Seideman, *Phys. Rev. Lett.*, 2004, **93**, 093004.

133 P. S. Christopher, M. Shapiro and P. Brumer, *J. Chem. Phys.*, 2005, **123**, 064313.

134 T. T. Nguyen-Dang, C. Lefebvre, H. Abou-Rachid and O. Atabek, *Phys. Rev. A*, 2005, **71**, 023403.

135 A. Biswas, M. Shapiro and P. Brumer, *J. Chem. Phys.*, 2010, **133**, 014103.

136 A. García-Vela, *J. Chem. Phys.*, 2012, **136**, 134304.

137 A. García-Vela, *J. Phys. Chem. Lett.*, 2012, **3**, 1941.

138 C. Sanz-Sanz, G. W. Richings and G. A. Worth, *Faraday Discuss.*, 2011, **153**, 275.

139 R. de Nalda, J. G. Izquierdo, J. Durá and L. Bañares, *J. Chem. Phys.*, 2007, **126**, 021101.

140 R. de Nalda, J. Dura, A. García-Vela, J. G. Izquierdo, J. González-Vázquez and L. Bañares, *J. Chem. Phys.*, 2008, **128**, 244309.

141 F. Krausz and M. Ivanov, *Rev. Mod. Phys.*, 2009, **81**, 163.

142 D. Xie, H. Guo, Y. Amatatsu and R. Kosloff, *J. Phys. Chem. A*, 2000, **104**, 1009.

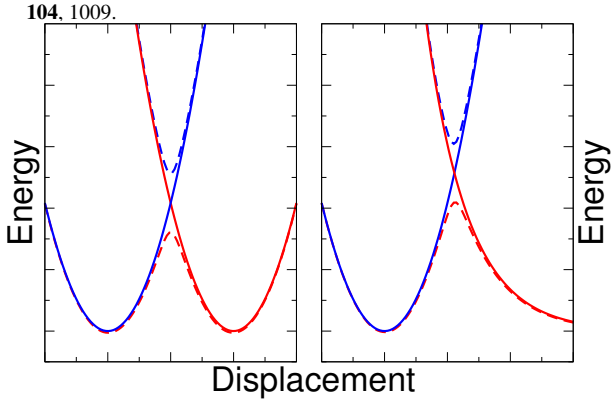

Fig. 1 Two cases of diabatic potential energy curves in the Floquet representation (solid curves) and the corresponding adiabatic potential energy curves (LIPs) (dashed curves). See the text for the details.

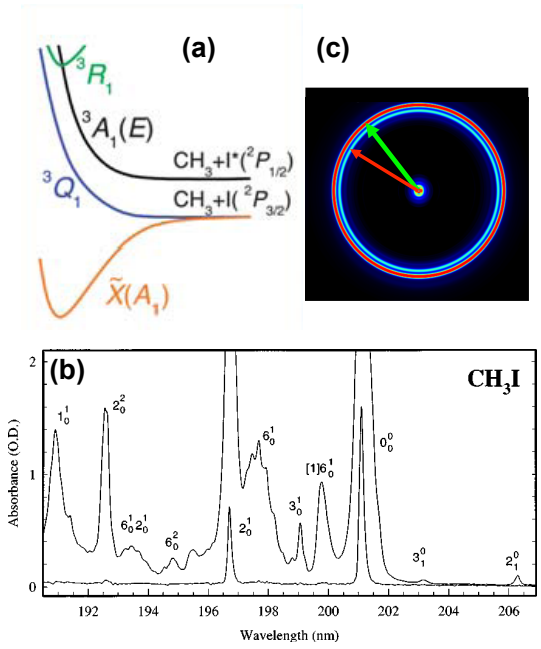

Fig. 2 (a) One-dimensional schematic cut of the states of CH_3I relevant for the *B*-band electronic predissociation process. Absorption in the region of 200 nm is dominated by transitions to the vibrational levels of the $^3R_1$ Rydberg state. These are lifetime broadened due to the crossing with the $^3A_1(E)$ state. This causes electronic predissociation in a picosecond time scale yielding $CH_3+I^*(^2P_{1/2})$. (b) Absorption spectrum of gas phase CH_3I in the region of 200 nm. The most intense peaks correspond to the 0_0^0 and 2_1^0 transitions [Reproduced from Ref. [128] with permission from American Physical Society]. (c) Abel-inverted CH_3 ion image (in false color) obtained upon *B*-band excitation of CH_3I to the ground vibrational level of the Rydberg $^3R_1$ state (pump center wavelength of 201.2 nm for the 0_0^0 transition) and later CH_3 resonant ionization through a (2+1) REMPI process at 333.5 nm, delayed by 10 ps. The main ring visible in the image (indicated with a green arrow) corresponds to the $CH_3(v=0)+I^*(^2P_{1/2})$ channel. A dimmer ring of lower fragment kinetic energy (indicated with a red arrow) corresponds to $CH_3(v_1=1)+I^*(^2P_{1/2})$, also visible due to the proximity of the 1_1^1 and 0_0^0 REMPI transitions in CH_3, both within the bandwidth of the femtosecond probe laser.

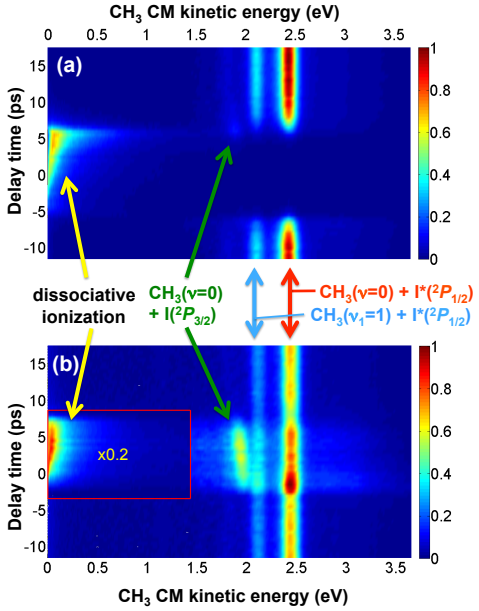

Fig. 3 (a) Intensity map showing the kinetic energy distribution of the CH_3 fragments resulting from *B*-band predissociation of CH_3I as a function of the time delay between the pump (201.2 nm) an the NIR control (800 nm) laser pulses. The control pulse is temporally stretched to obtain a FWHM of 3.9 ps with on-target intensities of about 5 TW cm^{-2}. CH_3 fragments are ionized with a 333.5 nm probe laser through (2+1) REMPI and detected in velocity map configuration. After Abel inversion and angular integration, CH_3 fragment kinetic energy distributions are obtained as a function of pump-control time delay. Application of the control field in temporal overlap with the pump pulse causes suppression of the main channels and the appearance of two new channels, multiphoton ionization and stimulated dump, indicated in the Figure. (b) Intensity map of CH_3^+ acquired under the same conditions as in (a) except that the pump laser has been tuned to the blue and is now centered at 200.5 nm. In this case, temporal overlap with the control pulse enhances the main channels and also the new stimulated dump channel.

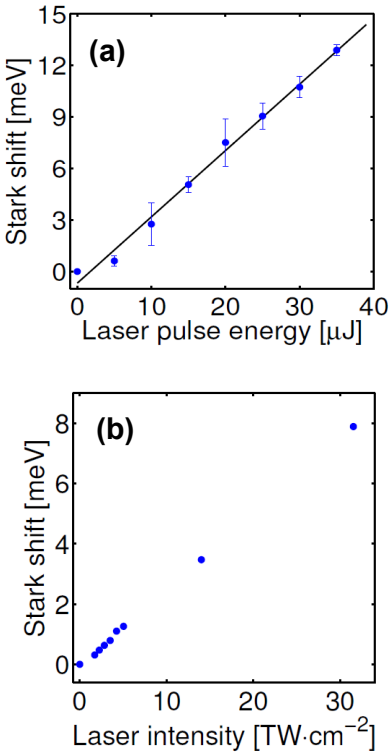

Fig. 4 Magnitude of the spectral Stark shift of the 0_0^0 transition of the *B*-band in CH_3I upon exposure to a strong NIR field plotted as a function of its intensity. (a) Measured Stark shift obtained by retuning the wavelength of the pump laser to the resonance for each value of the energy of the Stark pulse and linear regression of the data (solid line). Error bars correspond to one standard deviation. (b) Theoretical Stark shift as a function of laser intensity, calculated through the procedure indicated in the text [Reproduced from Ref. [126]]

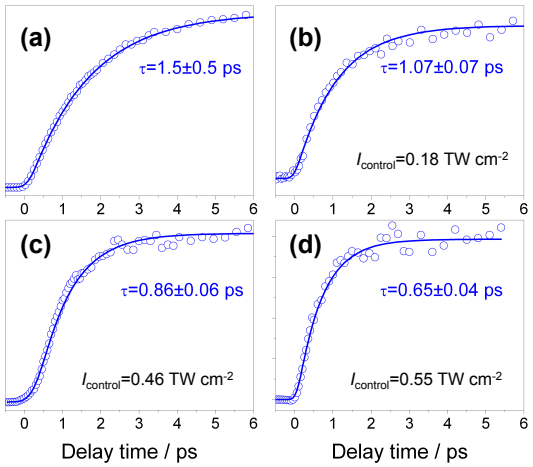

Fig. 5 Experimental transients showing the appearance of CH_3 fragments after *B*–band excitation of CH_3I. The transients correspond to the integrated CH_3 signal in the main $CH_3(v=0)+I^*(^2P_{1/2})$ channel. Fits to growing exponential functions yield lifetime values. The graphs show the transients, with their corresponding lifetimes, in the absence of an additional control field (a), and in the presence of a NIR field of a range of intensities ((b) to (d)). The delay time between the pump and control lasers is fixed at 1 ps, so that the pump pulse temporally overlaps with the beginning of the control pulse. Higher intensity fields cause substantial reduction of the measured lifetime.

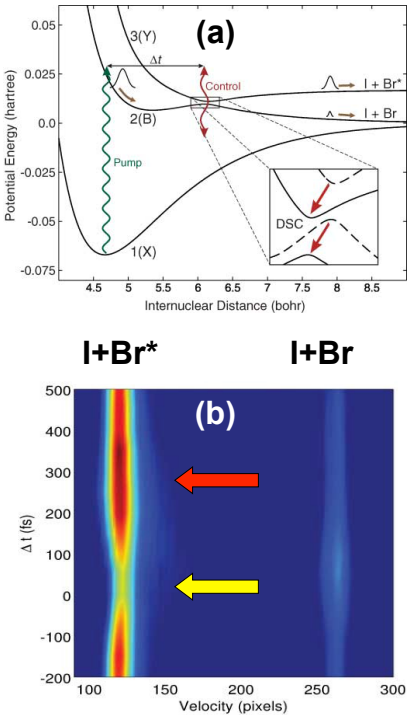

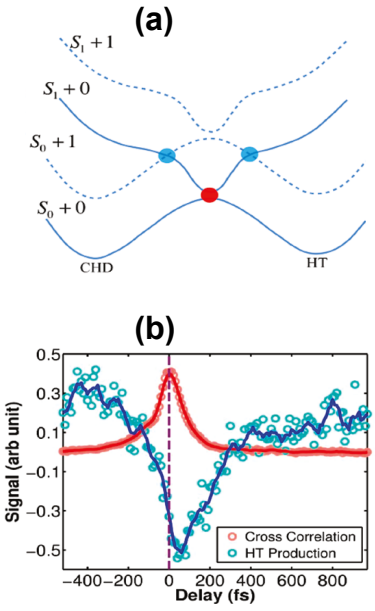

Fig. 6 Dynamic Stark control of the dissociation process in IBr. (a) The excited state wave packet traverses a nonadiabatic crossing, with two possible final states for the Br atom, Br($^2P_{3/2}$) or Br*($^2P_{1/2}$). An IR field dynamically modifies the adiabatic potential barrier during the reaction, altering the outcome. (b) Map of the velocity distributions of the iodine atoms as a function of the delay of the control pulse relative to the pump pulse. The Br*($^2P_{1/2}$) channel is suppressed (yellow arrow) near temporal overlap, and it is enhanced (red arrow) for delays in the region of 300 fs (see text for more details) [Reproduced from Ref. [102]].

Fig. 7 (a) Schematic representation of the states that are relevant to describe the ring opening of 1,3-cyclohexadiene (CHD), which can lead to isomerization into 1,3,5-hexatriene (HT). The solid lines are the bare energy levels (S_0 and S_1). The dashed lines are states dressed by one photon of the added NIR field (Floquet picture). The laser-induced conical intersections are indicated by the blue dots, and the molecular field-free conical intersection is indicated by the red dot. (b) Signal associated with the production of the HT species (blue circles) as a function of the delay of the control field, showing suppression at 50 fs [Figure reproduced from [112]].

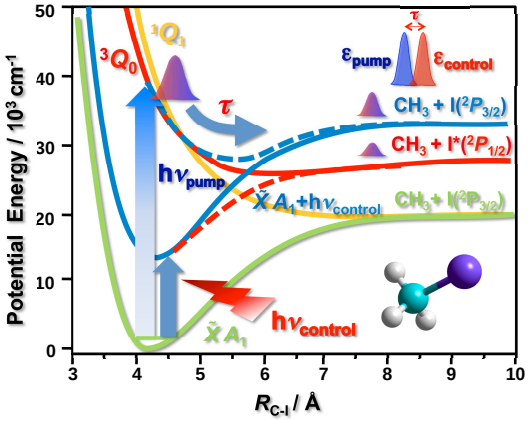

Fig. 8 Potential energy curves of the relevant electronic states involved in the photodissociation of CH_3I in the *A*-band along the R_{C-I} coordinate. The $^3Q_0$ (red line) and $^1Q_1$ (yellow line) potential energy curves are taken from Xie *et al.*[142]. The ground-state potential energy curve (green line) was calculated according to the *ab initio* method described in Ref.[113]. A pump pulse at 268 nm was used to prepare a wave packet in the $^3Q_0$ state. An intense ultrashort 804 nm control laser pulse was time delayed (τ) with respect to the pump pulse. This control pulse creates the LICI, here shown at the crossing of $^3Q_0$ and the $\tilde{X}\ ^1A_1$ ground electronic state, which has been shifted by the energy of the 804 nm photon (blue line). For sufficiently strong fields the control pulse also induces a strong modulation of the potentials around the LICI to create the corresponding LIPs (dashed red and blue lines) [Figure reproduced from[113]].

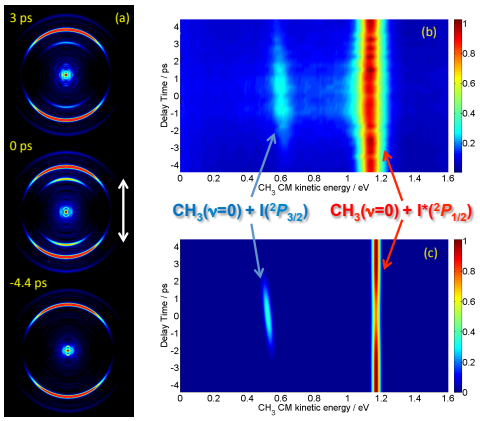

Fig. 9 Creation of a LICI in *A*-band dissociation of CH_3I. (a) Abel-inverted CH_3 images obtained upon 268 nm dissociation of CH_3I, for two values of the delay with respect to the added NIR control pulse (804 nm, 5 TW cm^{-2}, 3.9 ps FWHM). The CH_3 fragments are ionized by (2+1) REMPI with a further delayed pulse at 333.5 nm. In the top image, the NIR field is temporally separated from the pump pulse and causes no modification of the image (*i. e.* no effect over the reaction). This image shows the main channel corresponding to $CH_3(v{=}0)+I^*(^2P_{1/2})$ and the outer, weaker channel corresponding to $CH_3(v{=}0)+I(^2P_{3/2})$ that results from the intrinsic conical intersection of the $^3Q_0$ and $^1Q_1$ surfaces. In the bottom image, the NIR control field is temporally overlapped with the pump pulse, and a new contribution appears in the CH_3 image at lower kinetic energy. The double-sided arrow indicates the polarization axis of all three laser pulses. (b) Map of the kinetic energy distribution of CH_3 as a function of the delay between the pump and the control pulses, showing the new contribution at 0.6 eV during temporal overlap. This contribution is tilted, with lower kinetic energy release for longer delays. The interpretation of these results is that, in the presence of the control pulse, part of the wave packet is transferred back to the ground state through the LICI and dissociates into $CH_3(v{=}0)+I(^2P_{3/2})$ (see text for details).

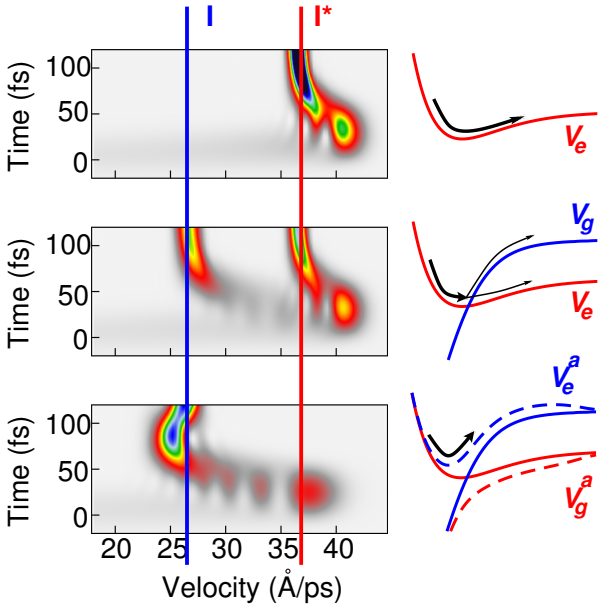

Fig. 10 Numerical simulations of the dissociation reaction in three different conditions with respect to the nature of the control field. Time-dependent fragment relative velocity distributions (left panels) obtained by integrating the time dependent Schrödinger equation using a 1D model within the Floquet representation for different control pulses with the pump pulse the same in all cases. The blue and red vertical lines indicate the final relative velocity of the fragments for the $CH_3(v=0)+I(^2P_{3/2})$ and $CH_3(v=0)+I^*(^2P_{1/2})$ channels, respectively, expected by energy conservation (that is, in the absence of the control pulse during the dynamics) after excitation with the pump pulse. (a) Top: No control pulse. (b) Middle: Long (3.9 ps FWHM) and moderately intense (5 TW cm^{-2}) top-hat control pulse. (c) Bottom: Long (3.9 ps FWHM) and strong (85 TW cm^{-2}) control pulse. The right panels show the molecular potentials and LIPs that explain the populations and shapes of the asymptotic fragment kinetic energy distributions. Arrows sketch the main contributing processes along with the shifts in the velocities that lead to the observed broadening and shifting of the asymptotic distributions; the thickness of the arrows represents the branching ratio between the different dissociation pathways.

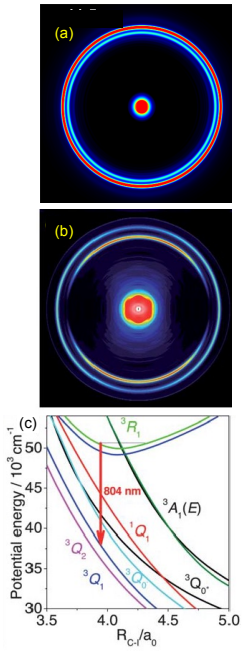

Fig. 11 Laser-induced dump process in the *B*-band dissociation of ground vibrational state of CH_3I. (a) CH_3 image obtained upon 201.5 nm excitation of CH_3I and (2+1) REMPI ionization of CH_3 at 333.5 nm. This image was obtained in field-free conditions, and the main ring corresponds to the $CH_3(v=0)+I^*(^2P_{1/2})$ channel. The weaker, more internal ring corresponds to CH_3 with excitation in the symmetric stretch mode, $CH_3(v_1=1)+I^*(^2P_{1/2})$. (b) Same as (a) except that this CH_3 image was obtained in conditions where the process takes place under the presence of an additional NIR field (804 nm, 4 ps FWHM, 0.55 TW cm^{-2}). New features include an enhanced central contribution, corresponding to low energy release processes of dissociative ionization, and an additional, well defined ring of parallel character and somewhat lower kinetic energy than the *B*-band contribution, which is attributed to transfer to the $^3Q_1$ state in a dump process and dissociation into $CH_3(v=0)+I(^2P_{3/2})$. (c) Scheme of the potential energy curves of CH_3I along the C–I distance coordinate relevant for the description of the dump process after *B*-band excitation. The mechanism is interpreted as a stimulated emission process transferring population from the quasibound $^3R_1$ state to the dissociative $^3Q_1$ state.

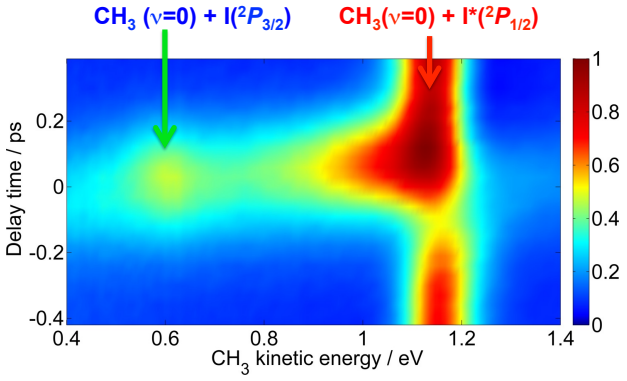

Fig. 12 Control of the kinetic energy release in the *A*–band CH_3I photodissociation using LIPS. The image contains a map of the CH_3 kinetic energy as a function of the time delay between a 268 nm pump pulse and a short, intense NIR (804 nm, 50 fs FWHM, 80 TW cm^{-2}) control pulse. In each case, CH_3 is ionized at a later time (about 30 ps) through a (2+1) REMPI process produced by a third short pulse centered at 333.5 nm. The main dissociation channel that appears at 1.15 eV kinetic energy (red arrow) corresponds to the $CH_3(v=0)+I^*(^2P_{1/2})$ channel. The kinetic energy distribution is unperturbed when the NIR control pulse is applied sufficiently before (negative times) or after (positive times) the interaction with the pump pulse. The introduction of the control pulse in the temporal vicinity of the pump introduces distortion in the kinetic energy distribution, which is bent towards lower values of the kinetic energy and it is also significantly broadened. This is described as the result of switching from the dressed to the bare states during dissociation. An additional channel at 0.6 eV (green arrow) is also detected, and can be understood as wave packet dynamics on the laser-induced potential that asymptotically yields $CH_3(v=0)+I(^2P_{3/2})$ (see text for further details) [Reproduced from Ref. [113]].

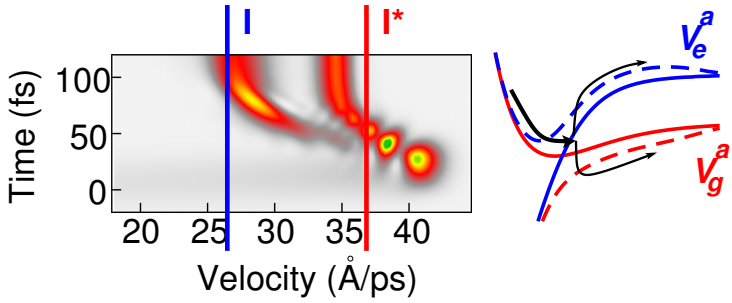

Fig. 13 Time-dependent fragment relative velocity distribution (left panel) obtained by integrating the time dependent Schrödinger equation using a 1D model within the Floquet representation. The blue and red vertical lines indicate the final relative velocity of the fragments for the $CH_3(v=0)+I(^2P_{3/2})$ and $CH_3(v=0)+I^*(^2P_{1/2})$ channels, respectively, expected by energy conservation (that is, in the absence of the control pulse during the dynamics) after excitation with the pump pulse. Strong (85 TW cm^{-2}) and short (50 fs FWHM) control pulse, time delayed by 60 fs with respect to the pump pulse. The right panel show the molecular potentials and LIPs that explain the populations and shapes of the asymptotic KEDs. Arrows sketch the main contributing processes along with the shifts in the velocities that lead to the observed broadening and shifting of the asymptotic distributions (see the text for the explanation); the thickness of the arrows represents the branching ratio between the different dissociation pathways.

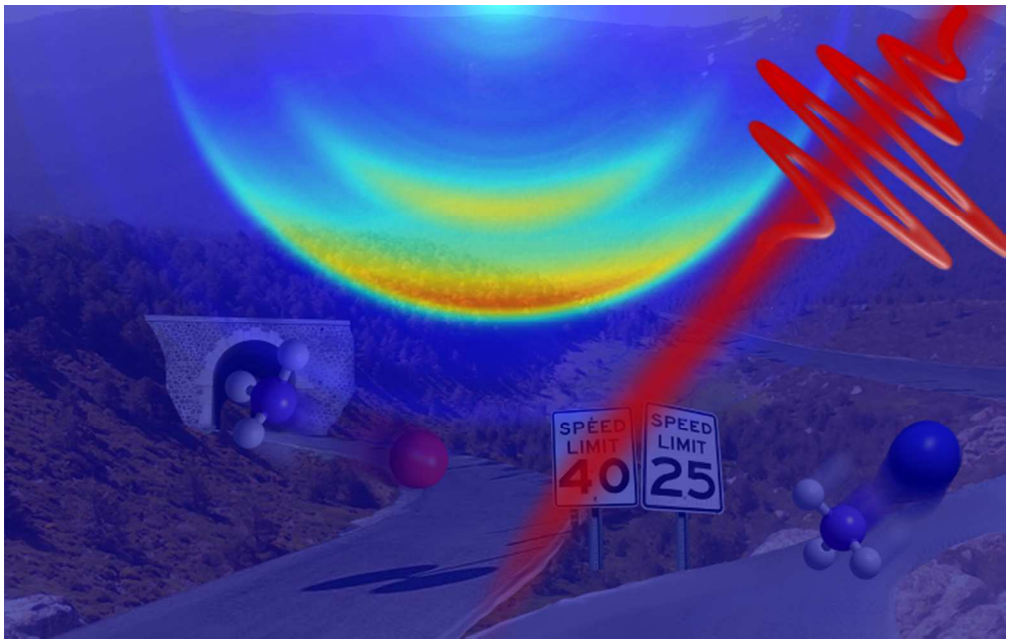

Intense ultrafast laser light is used as an additional reagent for steering photochemical reactions by dressing the potentials where the atoms move

Intense ultrafast laser light is used as an additional reagent for steering photochemical reactions by dressing the potentials where the atoms move